ULTRASONIC INSPECTION OF LIQUID-FILLED PRESSURE VESSELS USING PIEZOELECTRIC TRANSDUCERS

by

Jomah Alzoubi

A Thesis Submitted in

Partial Fulfillment of the

Requirements for the Degree of

Master of Science

in Engineering

at

The University of Wisconsin – Milwaukee

May 2024

ABSTRACT

ULTRASONIC INSPECTION OF LIQUID-FILLED PRESSURE VESSELS USING PIEZOELECTRIC TRANSDUCERS

by

Jomah Alzoubi

The University of Wisconsin – Milwaukee, 2024
Under the Supervision of Professor Nathan Salowitz

Automated structural inspection systems employing embedded sensing systems, known as structural health monitoring (SHM), have advanced greatly in recent decades. SHM enables online, real-time damage detection in hard-to-access locations, which can help prevent catastrophic failures. Some of the most advanced capabilities are based on elastic wave propagation in structures, with established capabilities of detecting and locating multiple forms of damage. Advanced capabilities of differentiating forms and extent of damage have recently been established. However, these capabilities are largely limited to simple structures like thin flat plates. Liquid-filled pressure vessels are common in aircraft and spacecraft but pose challenges to elastic wave-based SHM due to a combination of complex geometry and liquid contact that can alter the elastic wave propagation in the structure or transmit elastic waves itself. This work presents an investigation into the ultrasonic SHM of a small liquid-filled pressure vessel to build a physical understanding base of how the ultrasonic wave behaves under changing the states and the pressure under simulated damage. The results show that changing the states of the vessel from empty to full of water will directly affect the second arrivals packet (antisymmetric A_0) mode by diminishing the signals and reduction significantly the amplitude of the A_0 mode. Moreover, varying the pressure in the pressure vessel also reduces the amplitude of antisymmetric mode A_0 for both states empty and full of water.

To my family, and in loving memory of my father and my friend Yousef Shatnawi

TABLE OF CONTENTS

LIST OF FIGURES

LIST OF TABLES

ACKNOWLEDGEMENTS

I would like to express my sincere gratitude and appreciation to my advisor Professor. Salowitz, for his invaluable guidance, support, and mentorship throughout this work. His encouragement and insightful feedback have been shaping the direction and execution of this research. Professor Salowitz's contributions have significantly enriched this work, and I am truly grateful for the opportunity to learn from him.

Furthermore, I would like to extend my genuine appreciation to The Water Equipment and Policy Center (WEP) for their generous support in funding this project.

Additionally, I express heartfelt to my mother, brothers, my sister Amal, my wife Hebah, and my lovely kids (Eslam, Mohammad and Salma) for their unwavering support and encouragement throughout my academic journey.

Chapter 1

1.1.Introduction to Ultrasonic Structural Health Monitoring

Embedded, automated, real-time structural inspection techniques, known as structural health monitoring (SHM), have advanced greatly in recent years employing many physical principles including electrical impedance tomography, vibration monitoring, and thermography. Permanently embedding sensors into a structure of interest provides permanent access to hard-to-reach locations and consistency in coupling to the structure supporting automation of signal analysis and real-time inspection while the structure is in use.

One of the most capable forms of SHM is based on ultrasonic propagation of elastic waves. Ultrasonic SHM has been demonstrated to be capable of detection and location of many types of damage including cracking, erosion, corrosion, and adhesion of a foreign object on the surface of the structure. Advanced capabilities of identifying the form of damage and its extent have also been demonstrated. The sensitivity that makes ultrasonic SHM so capable is also one of the challenges to its use because the approach is also very sensitive to environmental effects like temperature changes.

There has been a recent interest in using active materials in structural health monitoring (SHM) due to their unique characteristic in sensing and actuating signals and based on the signal processing of the output signals from the PZT we can locate defects. Therefore, active materials such as piezoelectric materials were used to monitor structures by providing information about the state of structures. To achieve this goal, there are usually two ways to install the active materials on the structures: internally embedded or mounted on the surface structures.

Pitch-catch ultrasonic SHM typically employs an array of piezoelectric transducers (PETs) as actuators and sensors. These transducers strain when exposed to an electrical field (aka the reverse piezoelectric effect) and produce an electrical charge displacement when strained (aka the piezoelectric effect) [1]. A time-varying voltage is applied to the actuator

causing it to deform through its reverse piezoelectric effect. The deformation is transmitted into the host structure as a time-varying strain. Elastic waves propagate through the structure reflecting, refracting, and changing propagation modes when they encounter heterogeneities like damage. When the elastic waves arrive at the sensor, they strain the sensor. The piezoelectric property of the sensor produces a time-varying voltage that can be read with a data acquisition computer .

Lamb waves are used in thin-walled structures, it consists of a multimodal nature, where the velocity of each mode is dependent on the frequency content of the excitation signal and the thickness of the plate. In other words, lamb waves can be divided into two types of modes: symmetrical modes and anti-symmetrical modes. The modes are more sensitive for detection of surface defects, disbonding, and thickness damage [2]

1.2.Challenges

While significant progress has been made in recent research, challenges persist, such as the impact of material properties, geometric complexities, and the need for real-time inspection. For the Ultrasonic structural health monitoring of liquid-filled pressure vessels presents many challenges. The structure of the vessel itself is complicated with curved surfaces, joints, fittings, and other complexities. liquid filling the vessel constraints one surface of the structure altering potential elastic wave propagation modes, the liquid itself provides another potential path for elastic waves to propagate, and changes in pressure can cause changes in the elastic wave propagation and output signal.

Many techniques have been developed to overcome common complexities in ultrasonic SHM which will be leveraged for this new application. A primary complexity of elastic wave propagation in thin plates is the existence of multiple propagation modes and their dispersive nature, meaning that the speed of propagation is also frequency dependent. The introduction of time domain modulation introduces frequency content that causes the propagating waves

to distort. The ability to model this distortion is itself an area of active research. Equations and dispersion curves for Lamb wave propagation in thin flat plates were developed by Horace Lamb in 1917 but require numerical solutions and didn't see much use until recently [3]. Finite element modeling is capable of accurately modeling the wave propagation but requires extremely fine meshes that make modeling of large and complex structures prohibitive.

Changes in the output signal can be interpreted to identify and locate changes and damage in the structure. Because this approach compares to a baseline for the structure, it has the potential to accommodate complex geometries but assumes is insensitive to pre-existing conditions. The initial data is taken in a state where the structure is assumed to be 'pristine,' any existing damage or defects will not be detected, though the growth of such conditions can be sensed. While many advanced capabilities have been developed using this approach, theory and capabilities are largely limited to simple, (nearly) flat, thin plate-type structures [4].

1.3.Thesis Overview

This thesis comprises seven chapters. The first chapter offers a brief introduction to ultrasonic structural health monitoring, outlining its challenges and methodologies. The second chapter delves into a comprehensive background and literature review concerning ultrasonic inspection across various structures, exploring different modes of wave propagation. It also presents recent research on ultrasonic inspection of pressure vessels and outlines the scope of the thesis.

The third chapter details the testbed and experimental setup, along with the methodologies employed. It discusses the actuation and sensing signals and the selection of PZT size and specifications. Additionally, it covers the calculation of the system's natural frequency using different methods such as Manual, Chirp, and Welch. Chapter four addresses

the utilization of a damage index in structural health monitoring (SHM) and the techniques applied for signal smoothing and processing in sensing signals such as Multi-level Discrete Wavelet Transform (DWT) decomposition. Moreover, the defect location algorithm has been formulated, incorporating (ToF) and the damage index (DI).

Chapter five explores the impact of different states (empty and filled-water states) on ultrasonic inspection, alongside examining the response of sensing signals to simulated damage. Chapter six digs into examining the influence of pressure on the pressure vessel under varying conditions: empty and filled with water, with and without simulated damage. The investigation involves calculating damage indexes, including RMSD, CCD, and NSE, to analyze the impact of simulated damage on the sensing signals.

In chapter seven, the exploration focuses on the damage localization algorithm and determining the optimal number of transducers required to cover the pressure vessel. Chapter nine, the concluding chapter, offers a summary of the key findings of the thesis and outlines for future research.

Chapter 2

2.1. Background and Literature Review

Pressure vessels play a critical role in various industries, including petrochemical, nuclear, and aerospace, where they are subjected to extreme conditions (high pressure and temperature). Ensuring the structural integrity of these vessels is paramount to prevent catastrophic failures that can lead to severe consequences. Ultrasonic inspection has emerged as a key non-destructive testing (NDT) method for assessing the internal integrity of pressure vessels. This literature review explores the latest research and advancements in ultrasonic inspection techniques for pressure vessels.

Ultrasonic testing relies on the propagation of high-frequency sound waves through the material, with echoes analyzed to identify defects or irregularities. Traditional ultrasonic methods, such as pulse-echo and through-transmission, have been widely employed for system inspection. However, recent research focuses on enhancing these techniques and introducing innovative approaches to improve accuracy, reliability, and efficiency [5].

Guided wave ultrasonics have gained prominence for their ability to inspect large areas of the structure from a single point. Research in this area focuses on optimizing guided wave techniques to detect and characterize defects in complex geometries and multi-layered structures. Signal processing algorithms are being developed to improve the accuracy of defect localization and sizing, addressing challenges posed by various materials and structure configurations [6]

Recent literature highlights the development of innovative inspection protocols that combine multiple ultrasonic techniques. For example, the integration of conventional pulse-echo methods with guided wave ultrasonics provides a more comprehensive assessment of pressure vessel integrity. These hybrid approaches aim to overcome limitations associated with individual techniques and enhance the overall inspection performance [7]

The integration of machine learning and data analytics in ultrasonic inspection research is a notable trend. Advanced signal processing algorithms and artificial intelligence models are being applied to analyze ultrasonic data more efficiently, enabling automated defect detection, classification, and predictive maintenance. These developments contribute to reducing inspection time and enhancing the reliability of pressure vessel assessments [8]

While significant progress has been made in recent research, challenges persist, such as the impact of material properties, geometric complexities, and the need for real-time inspection. Future directions in ultrasonic inspection for pressure vessels include the exploration of novel sensor technologies, further integration of artificial intelligence, and the development of standardized protocols to ensure consistency and reliability across industries [9].

2.2. Ultrasonic Waves for Damage Detection

Ultrasonic waves are widely used for damage detection in various materials and structures. This non-destructive testing (NDT) technique is based on the principles of ultrasound, where high-frequency sound waves are utilized to inspect the internal structure of a material without causing any damage. Here's an overview of how ultrasonic waves are used for damage detection:

2.2.1 Lamb waves

Often referred to as Lamb waves, can be effectively used for detecting joint defects in materials. Lamb waves are guided ultrasonic waves that propagate in plates and pressure vessel and can be either symmetric or antisymmetric in nature [4]. Antisymmetric Lamb waves have displacement components that are antisymmetric about the plate thickness. Antisymmetric Lamb waves can be generated using specialized transducers or other wave generation techniques, piezoelectric transducers are commonly used to generate Lamb waves in plates, antisymmetric Lamb waves is the theory spans and connects from full body flexural waves to surface Rayleigh waves, the flexural body waves are sensitive to the full thickness,

while Rayleigh are not. Antisymmetric can propagate through structure at different modes, such as the A_0 mode (fundamental antisymmetric mode), which is commonly used for defect detection [10].

2.3. Ultrasonic inspection of pressure vessel

Lugovtsova et al. [11]studied the Type III gas cylinder used by firefighters, The vessel consists of a 2 mm aluminium liner and Glass fibre-reinforced plastic (GFRP), by utilization of guided ultrasonic waves as a non-destructive means of assessing the structural health of composite pressure vessels. These waves have shown promise in detecting various damage types, including cracking in the metal liner, fiber breaks, and composite matrix delaminatio and the ability to identify these issues without causing additional stress to the material. Through presenting simulation results obtained through FEM, they offered a comprehensive analysis of wave modes and their interaction with different flaw types. They have findings highlight key considerations such as appropriate wave modes, defect-mode interactions, necessary excitation methods, and suitable sensor configurations. These insights are paramount for the effective design and implementation of a reliable SHM system for composite pressure vessels.

Fucai et al. [12] used cylindrical pressure semi-elliptical heads/caps on each end filled with water. They focus on analyzing the dispersive features of guided waves in the cylindrical structure, considering geometric similarity. Three types of guided wave modes – longitudinal, torsional, and flexural modes – are studied through theoretical methods, and dispersion curves are calculated. The study optimizes the central frequency and wave parameters of the incident wave based on analyses and experimental signals. Additionally, the impact of the contained liquid on guided wave propagation, particularly the L(0, 2) mode, is investigated to minimize energy leakage. Their research employs analytical methods, Finite Element Analysis (FEA), and experiments to explore the propagation characteristics of guided waves in the pressure vessel.

The study [13] introduces an ultrasonic method using shear horizontal (SH) waves to assess surface damage in fatigued materials, specifically pressure vessel made from CrMoV and 12Cr alloy steel. Through interrupted fatigue testing, the research finds that increasing fatigue damage correlates with longer propagation time and decreased wavelet amplitude. Waveform modulation analysis yields reliable estimations, with 97% confidence for 12Cr steel and 95% for CrMoV steel. The study concludes that SH ultrasonic waves can nondestructively determine fatigue damage in in-service components.

[14] This study introduces a method for inspecting the welded joint between the head and thick-walled nozzle of Multi-layered Steel Vessels (MLSV) used in high-pressure hydrogen storage for refueling stations. The proposed approach involves inserted curved surface coupling phased array ultrasonic inspection (PAUI). The study systematically analyzes various inspection parameters to address challenges like far detection distance, wide detection area, and material attenuation. Optimized parameters and scanning methods are determined, guiding the creation of a corresponding probe. An experimental test block validates the effectiveness of the proposed PAUI method for MLSV welded joint inspection.

2.4. Scope of the Thesis

This work presents an initial investigation into the ability to perform automated ultrasonic inspection of liquid-filled pressure vessels using embedded sensing systems. Liquid-filled liquid pressure vessels are a common and core structural component of spacecraft. Liquid-filled pressure vessels often operate under extreme conditions such as high temperature and pressure with potentially catastrophic consequences if they fail. Even a simple release of liquid could have severe consequences. The work also studies the ultrasonic inspection at different states (empty and full of water vessel) and the effect of the pressure on the ultrasonic waves. In addition to that the damage indexes are calculated for temporary damage like sticky patches and magnetic objects.

Chapter 3

3.1.Testbed

This work is pursuing an experimental approach with physics-based analysis to explore the ability to use pitch-catch ultrasonic SHM techniques for damage detection on a small liquid filled pressure vessel. A 6 liter, on-demand water heater tank was donated by AO Smith for use as a testbed shown in Fig. 3.1. This tank has a steel exterior lined with zircon ($ZrSiO_4$) to prevent corrosion. The water tank has three holes, two of which are threaded and the same diameter (outer diameter is 0.75 Inches) which is used as an inlet and outlet for water. The 3rd hole is significantly larger and is used to insert the heating element(coils). The water tank has a cylindrical shape with semi-elliptical heads, the diameter of the tank is 10 inches, and the height is 6.5 inches.

Figure 3. 1: Water tank mounted on support with PZTs attached.

Steps are being taken to control boundary conditions and environmental effects of the system. To ensure consistent boundary conditions, the tank is being mounted on a frame with consistent/controlled contact points. Similarly, the tank will be sealed except for a single filling pipe and pressure fixture. Experiments will be performed initially on the empty tank to help identify changes in signals due to the introduction of water. For the ‘in-use’ state the

tank will be filled with water with the only potential air pocket in the connecting pipe to ensure consistent boundary conditions in the tank. To limit potential environmental effects, the internal pressure and temperature will be monitored and controlled using sensors and valves in the fill pipe.

3.2.Method Used.

Pitch-catch ultrasonic SHM typically employs an array of piezoelectric transducers (PZTs) as actuators and sensors. Transducers strain when exposed to an electrical field (aka the reverse piezoelectric effect) and produce an electrical charge displacement when strained (aka the piezoelectric effect) [1]. A simplified version of the pitch-catch method is shown below in fig 3.2 where the transmitter on the left propagates an ultrasonic wave through the structure to the receiver on the right.

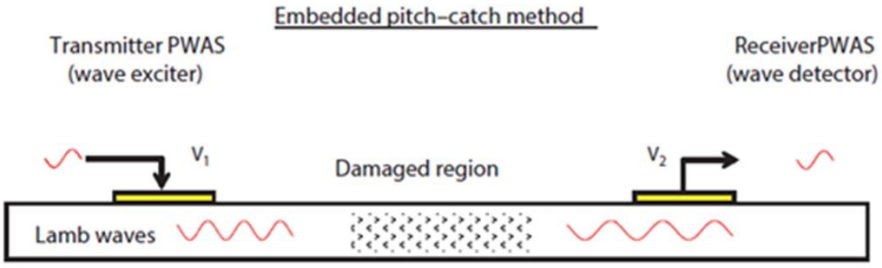

Figure 3. 2: Pitch-catch method [4]

Changes in the ultrasonic wave propagated indicate damage present and can be further analyzed to quantify the severity and location of the damage. However, Piezoelectric transducers have been mounted on the exterior surface of the water tank and used to actuate and sense elastic waves. Initially an array of common actuation signals will be investigated to support analysis of resonant and optimal frequencies. Output signals produced in various conditions and with various combinations of actuators and sensors will be analyzed based on physical models of the system and compared to each other to ensure understanding of the system and guide re-design and optimization.

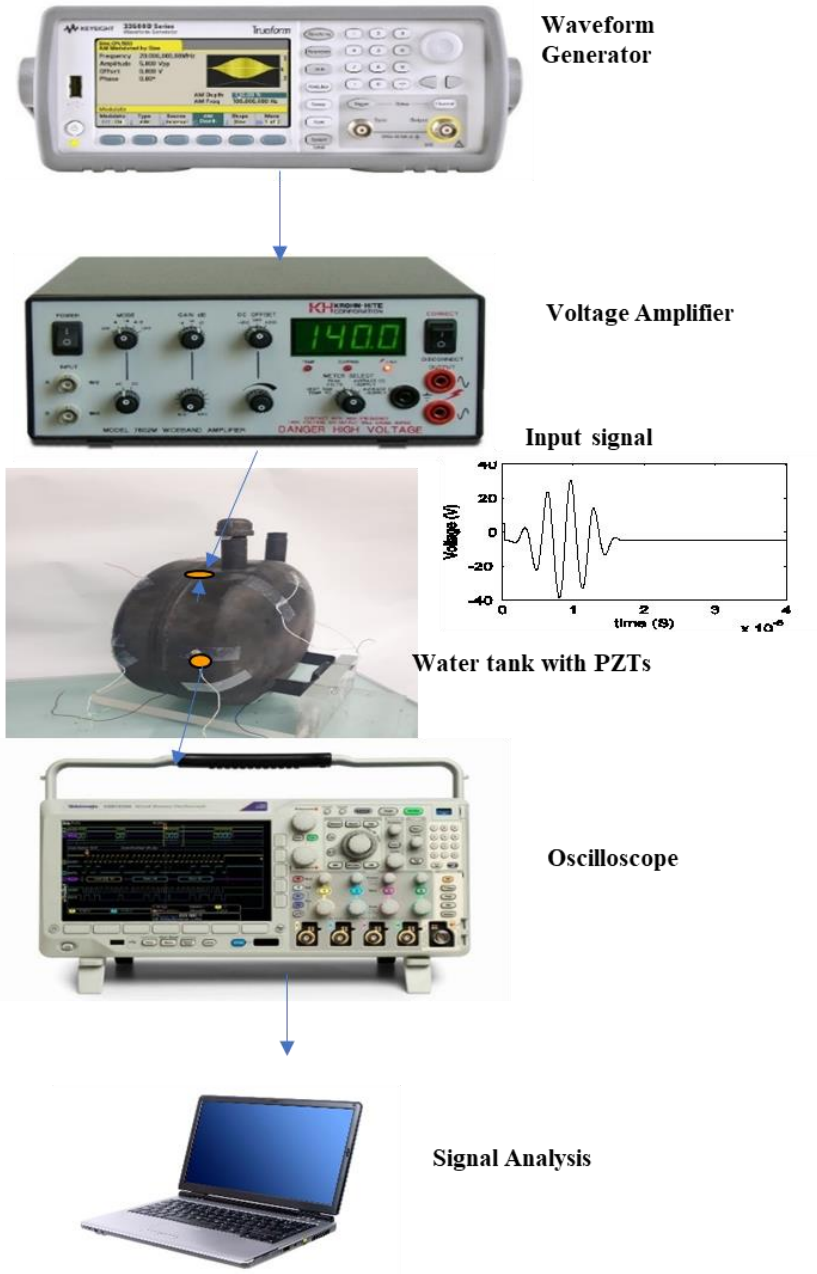

Figure 3. 3:Ultrasonic SHM setup

3.2.1. Actuation signal

The PZT actuator was driven by an actuation signal consisting of a 5-peak tone burst, Hann windowed centered at 300 kHz. The signal has been amplified from 9 V to 55 V using an amplifier due to the signal generator's maximum voltage being less than 10 V. Fig 3.4 illustrates the actuation signal.

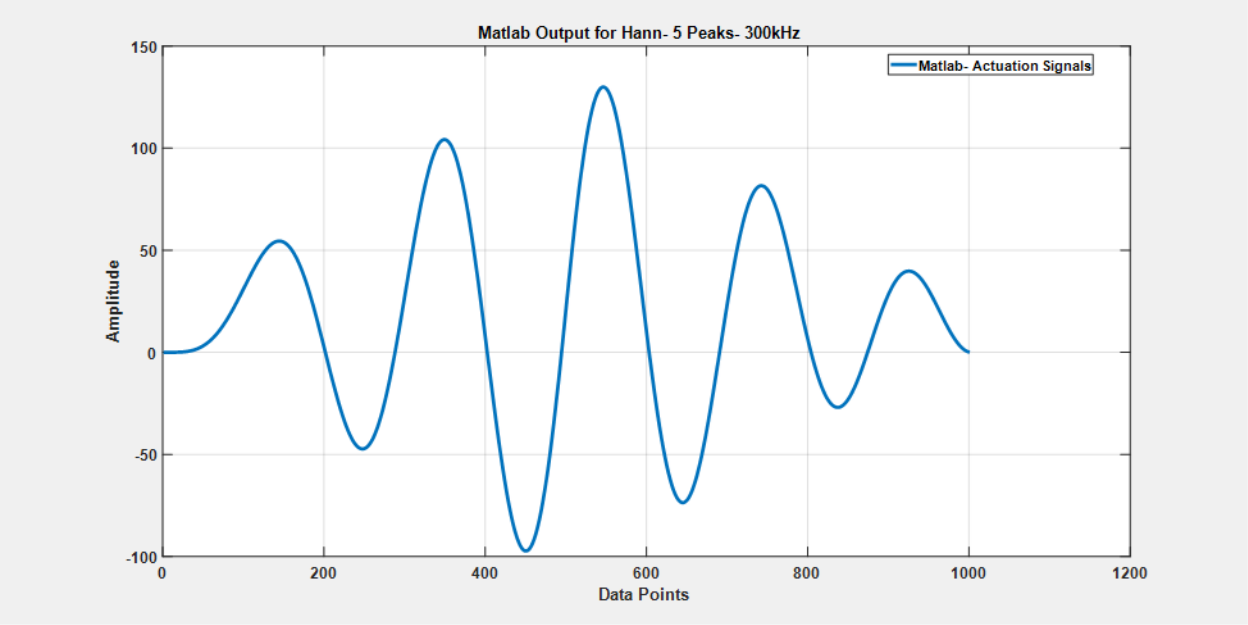

Figure 3. 4: MATLAB output of the actuation signal.

3.2.2. Sensing signal

The response of a PZT (Piezoelectric) sensor refers to its reaction or output when subjected to an external stimulus, typically mechanical or acoustic in nature. PZT sensors utilize the piezoelectric effect, where certain materials generate an electrical charge in response to applied mechanical stress or vibrations. When a PZT sensor is exposed to mechanical deformation or vibrations, the piezoelectric material within the sensor generates an electric charge proportional to the applied force. This electric charge is then measured or recorded as the sensor's response. However, the sensor response has a distinctive feature to analysis the response such as Time of Flight (ToF), changing in modes shapes (Symmetric S_0 and Anti-symmetric A_0), changing in amplitudes, and the angle shift on signals. Fig 3.5 shows the feature of the PZT sensor response.

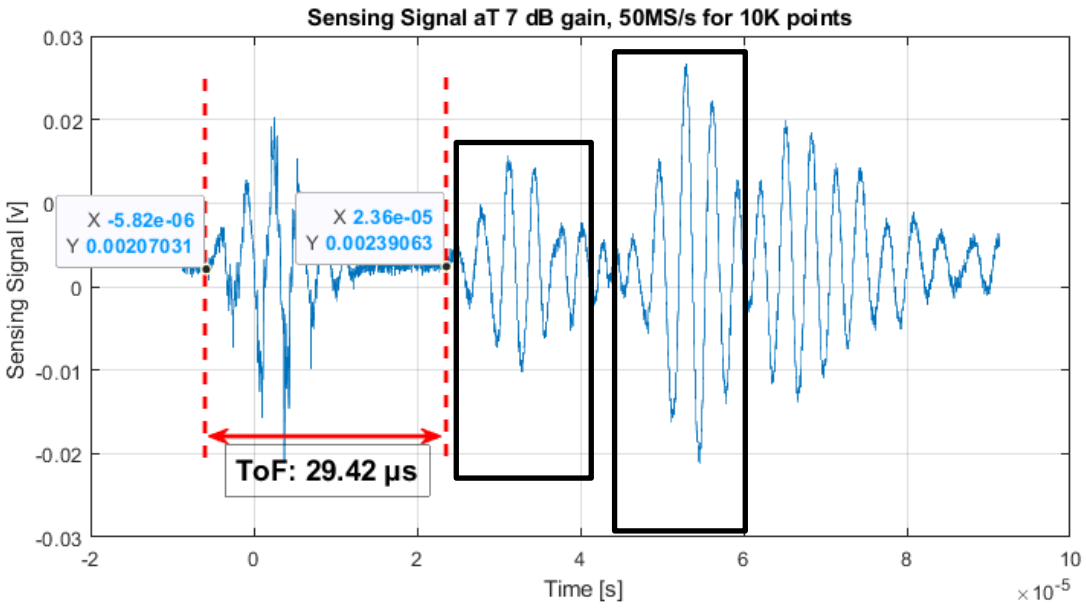

Figure 3. 5: Sensing Signal

3.2.2.1.Time of Flight

ToF refers to the time taken for an ultrasonic wave to travel from the start of actuation to start of initial arrival (S_0) on the sensing signal. By measuring the ToF, can help us to localize the defects on the structure and determine the speed of the signal (if the distance between the actuator and sensor is equal to 0.13 m then the speed of the wave in structure will be equal:

$$\boldsymbol{Velocity = \frac{Distance}{Time} = \frac{0.13}{29.42 * 10^{-6}}\ \frac{m}{s} = 4418\ \frac{m}{s}}$$

3.2.2.2. S_0 and A_0 Modes

The "S" in S_0 stands for "Symmetric," and the "0" indicates that it is the fundamental symmetric Lamb wave mode, where the "A" in A_0 stands for "Anti-symmetric," and like S_0, the "0" indicates that it is the fundamental antisymmetric Lamb wave mode. These Lamb wave modes play a significant role in ultrasonic testing because they have different characteristics and sensitivities to defects or irregularities in the material. The S_0 mode is

faster and often more sensitive to surface-breaking defects, while the A_0 mode is slower and can propagate through the thickness of the material,

3.3. PZT Size and specification

"PZT" stands for Lead Zirconate Titanate, which is a type of ceramic material known for its piezoelectric properties. Piezoelectric materials generate an electric charge in response to mechanical stress and vice versa, making them useful in various applications, including sensors, actuators, and transducers. The constitutive equations for piezoelectric materials in 3-dimensional strain charge form is commonly presented in the form of equations 1 and 2.

$$\boldsymbol{\varepsilon = S\,\sigma + d^t\,E} \qquad (\mathbf{1})$$

$$\boldsymbol{D = d\,\sigma + \varepsilon^t\,E} \qquad (\mathbf{2})$$

Where, ε = Strain[6x1], S = Compliance[6x6], σ = Stress[6x1], dt = Piezoelectric coupling coefficient (t = transpose) [3x6], E = Electric field[3x1], D = Electrical charge displacement[3x1], εt = Total permittivity. Lead Zirconate Titanate (PZT) is one of the most common piezoelectric materials with distinct structure and symmetry in these coefficients. Surface-mounted PZTs, polarized in the 3 directions, perpendicular to the surface produce strong actuation and sensing parallel to the surface, governed by the d31 coefficient because they can push against structure in this direction. These same materials will often produce weaker actuation perpendicular to the structural surface because they only have their own mass to react against.

The PZT transducer has been selected based on specific properties such as capacitance resonance frequency, couple wavelength and the coupling frequency. Therefore, the APC 850 disk shape has been used with thickness 1 mm, diameter 6 mm.

Table 3. 1: PZT properties and equations

PZT Properties	Description
Capacitance	$\boldsymbol{C = \frac{\epsilon * \pi * d^2 * K_{33}^T}{4 * t}}$
Resonance Frequency	$f_r = \frac{N_p}{2r}$
Wavelength Propagation	$\boldsymbol{\lambda = 2d = \frac{v}{f_c}}$
Coupling Frequency	$\boldsymbol{f_c = \frac{v}{\lambda}}$

Where:

ϵ: ,K_{33}^T: (Relative Dielectric Constant for APC 850) = 1900,

d: $PZT\ diameter\ (m)$, t: $PZT\ thickness\ (m)$,

N_p: $Is\ the\ radial\ \ frequncy\ constant;\ for\ the\ APC$ 850 = 1980

r: $is\ the\ PZT\ radius$, $wave\ speed\ v$ $= 4418 \frac{m}{s}$, Wavelength(λ)

Consequently, the specifications for our work based on the equations above will entail PZTs with the following parameters: thickness of 1 mm, diameter of 6 mm, resonance frequency of 330 kHz, wavelength of 12 mm, coupling frequency of 368 kHz, and capacitance of 475 pF.

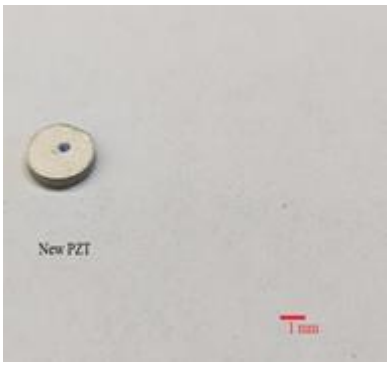

Figure 3. 6: Piezoelectric transducer size

3.4.Natural Frequency of the Pressure Vessel

The initial analysis has been conducted on an empty tank to find the natural frequency of the tank. Finding the natural frequency of a system is crucial in various engineering and scientific fields, as it provides valuable insights into the dynamic behavior and response of the system. However, many methods are used to identify the natural frequency of the system such as manual, welch, and chirp methods.

3.5. Manual Method

In this method, the sinewave has sweeping manually from 100 kHz to 500 kHz; the maximum power was -68 dBm happens at 440 kHz as shown in figure 4. The lowest strength power was -110 dBm which happened at 100 kHz. There are many strong peaks at different frequencies such as 320, 390,440 and 480 kHz. The frequencies associated with the identified peaks may provide estimates of the natural frequencies of the system. From fig 3.7 we can notice that the natural frequency of the system has occurred at 320, 390,440 and 480 kHz.

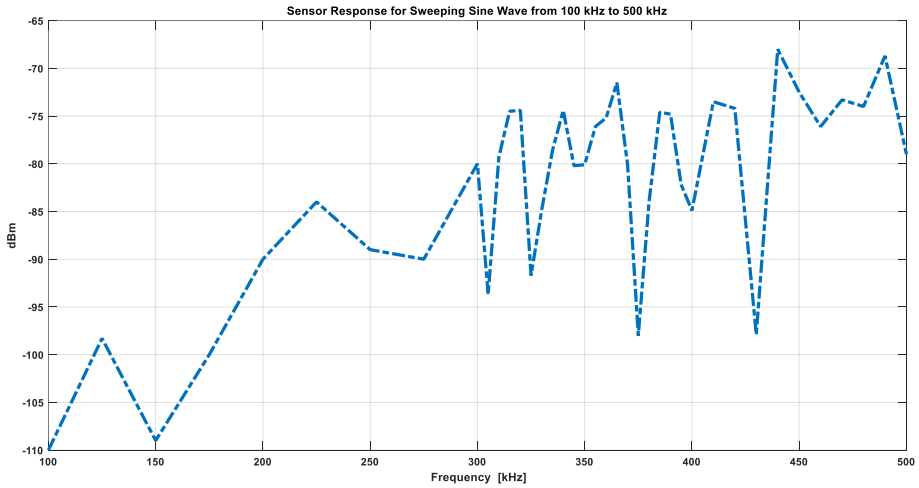

Figure 3. 7: Manual Method

3.6.Welch Method

Welch method is a technique for estimating the power spectral density (PSD) of a signal, which can indirectly provide information about the natural frequency of a system. The PZTs are actuated by using (Sine wave + noise) as shown in fig 3.8, the response of three

PZTs sensors has been recorded and tabulated in table. Table 3.2 and fig 3.9 present the power of the four peaks on dBm for the three sensors' responses.

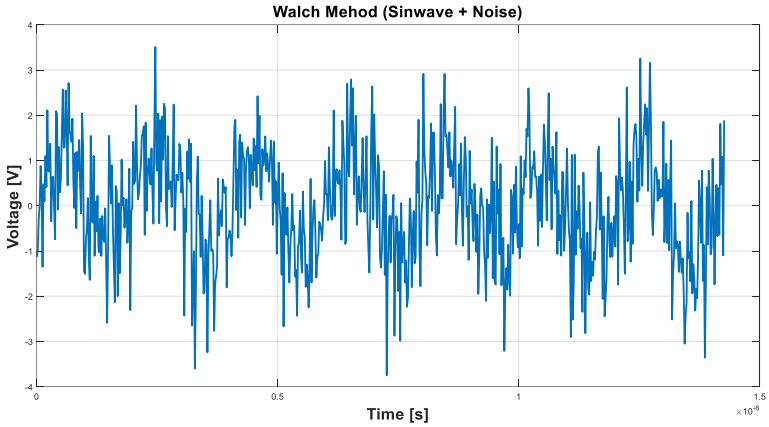

Figure 3. 8: Actuation signal for the Welch method

Table 3. 2: Power of the peaks on dBm for the three sensors' response

Frequency [kHz]	Sensor 1 [dBm]	Sensor 2 [dBm]	Sensor 3 [dBm]
310	-87	-98	-90
390	-87	-92	-88
440	-96	-89	-91
480	-84	-91	-84

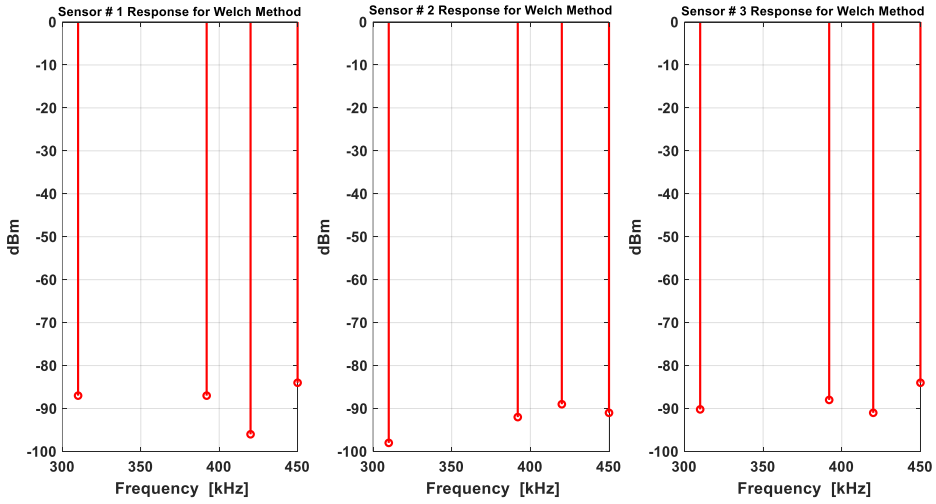

Figure 3. 9: Power of the peaks on dBm for the three sensors' response

The manual method and Welch method produce the same results, both methods show that they have peaks appearing on 320, 390, 440 kHz. The maximum power for the manual method was at 440 kHz, while the maximum power for the welch method differed based on the location of the sensor, but still had strong four peaks at 310, 390 and 440 kHz, compared with other frequencies.

3.6.1. Chirp Method

The chirp method also can be used for estimating the frequency content of a signal, and it can be applied for identifying natural frequencies in a system. The basic idea behind the Chirp method is to analyze a signal with a variable frequency component, which is often called a chirp signal. Generate a chirp signal, which is a signal that varies in frequency over time. The frequency sweep should cover the expected range of natural frequencies in the system.

The sensor response has been recorded for the frequency range of 100 to 500 kHz as done in the previous analyses using the manual and welch methods**.** Fig 3.10 below shows the Frequency (Hz) vs Sensor Response (dBm).

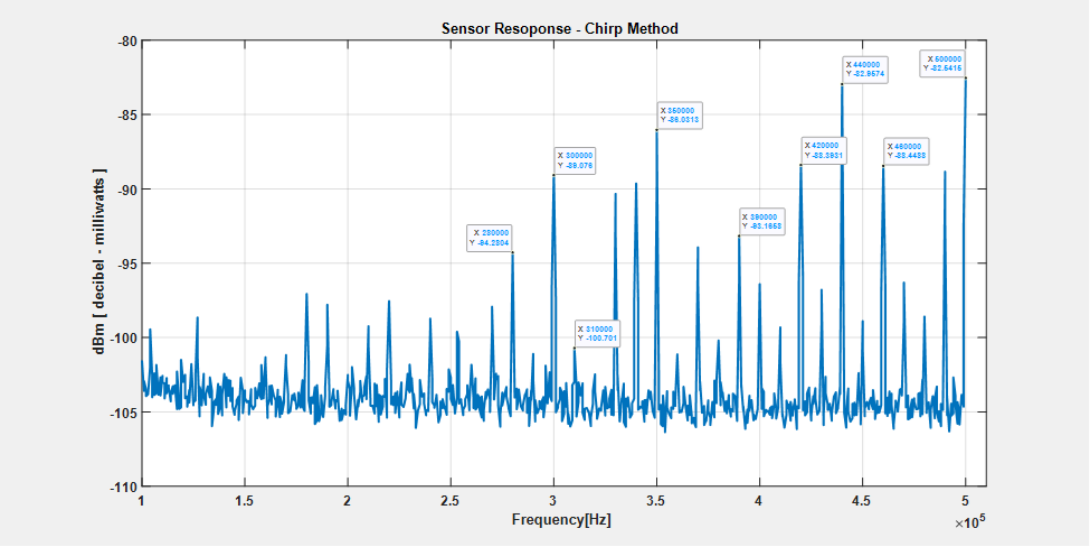

Figure 3. 10: Sensor response using the Chirp method.

The sensor response reached its highest value at 440 kHz, aligning with the peak sensor response identified in the manual analysis Furthermore, additional prominent peaks at

390 kHz, 420 kHz, and 480 kHz were observed using the chirp method, consistent with the peaks detected in both manual and Welch analyses. However, distinctive differences emerged in the chirp method's sensor response, revealing peaks at 280 kHz, 300 kHz, and 500 kHz that were absent in the other two methods. Additionally, the response at 310 kHz in the chirp method exhibited a weaker intensity compared to the responses at this frequency in the manual and Welch analyses.

3.7.Summary and Conclusions

In this chapter, the testbed and the pitch-catch method are discussed in detail, a small liquid filled pressure vessel. A 6 liter, on-demand water heater tank is the boundary conditions and environmental effects of the system are control such as temperature and pressure, to ensure consistent boundary conditions. The e pitch-catch method is implemented through using piezoelectric transducers that are mounted on the exterior surface and using typical ultrasonic SHM setup. The natural frequency for the pressure vessel has been identified through manual, Welch, and Chirp methods. The three methods produce the same results and confirm that natural frequencies of the pressure vessel have appeared on 310, 390, 440, and 480 kHz.

Chapter 4:

4.1. Damage Index

The Damage Index (DI) represents a scalar quantity, which indicates the disparity between two signal contents from the same entity through using statistical methods [15]. The sensitivity of the damage index is heavily dependent on signal characteristics and the statistical methodology employed for signal processing. The DI Typically used for detecting the presence of damage and evaluating its extent, the damage index can also pinpoint the location of damage by calculating the index at various locations within a structure. The table 4.1 show the most DI used on SHM [16].

Table 4. 1: Damage index methods

Damage Index (DI)	Description
Root mean square deviation (RMSD)	$RMSD = \sqrt{\frac{\sum_{t=1}^{n}(V_{Pristine}(t) - V_{Damage}(t))^2}{\sum_{t=1}^{n}(V_{Pristine}(t))^2}}$
Normalized signal energy (NSE)	$NSE = \frac{\sum_{t=1}^{n}(V_{Pristine}(t))^2 - \sum_{t=1}^{n}(V_{Pristine}(t))^2}{\sum_{t=1}^{n}(V_{Pristine}(t))^2}$
Correlation Coefficient Deviation (CCD)	$CCD = 1 - \frac{Cov((V_{Pristine}, V_{Damage})}{\sigma_{Pristine}\,\sigma_{Damage}}$, $Cov\big((V_{Pristine}, V_{Damage}\big) = \frac{1}{N}\sum_{i=1}^{N}(V_i - \bar{V})_{Pristine}\ (V_i - \bar{V})_{Damage}$
Peak-to-peak amplitude (PTPA)	$PTPA = \frac{PTPA_{Pristine}}{PTPA_{Damage}}$

In table 4.1, $V_{Pristine}$ is the pristine state at the t[th] measurement point, V_{Damage} is the comparison signal (damaged state) at t[th] measurement point; t is the time at measurement point, $\sigma_{Pristine}$ and σ_{Damage} $are\ the\ standard\ deviation\ of$

$(V_{Pristine}\ and\ V_{Damage})$, $(\bar{V})_{Pristine}\ and\ (\bar{V})_{Damage}$ are the mean of the pristine signal and the damage signal, respectively.

4.2. Signal Smoothing and Processing.

Smoothing a signal typically refers to the process of reducing noise or fluctuations in a data signal to reveal underlying trends or patterns more clearly [17]. There are various techniques for signal smoothing, such as moving averages and low-pass filters. However, [4] the author points out the key solution to removing the sharpness in the signals in the ultrasonic inspection by using Digital Filters such as (multi-level DWT decomposition Butterworth, Chebyshev I, Chebyshev II, and Elliptic). In this work we use DWT filter after noticing that the signal becomes sharper and distorted after a specific time, approximately 120 microseconds.

Multi-level Discrete Wavelet Transform (DWT) decomposition is a signal processing technique used for analyzing and processing signals, such as images or time-series data. It is based on the wavelet transform, which decomposes a signal into different frequency components, each representing a different level of detail or approximation [18].

In the first stage, the DWT initially applies the decomposition of the original signal into approximation coefficients (low-frequency information) and detail coefficients (high-frequency information) at different scales or levels. Once we have the DWT coefficients, we can apply filtering to remove or attenuate unwanted frequency components [18]. This can be done by zeroing out or reducing the amplitude of certain coefficients in the transformed domain. However, applying the DWT decomposition filter to the sensing signal has effectively diminished signal sharpness beyond 120 microseconds. This improvement facilitates the analysis of structures linked to both symmetrical and unsymmetrical modes even if the modes appear after the 120-microsecond threshold. Fig 4.1 shows the sensing signals before and after applying DWT .

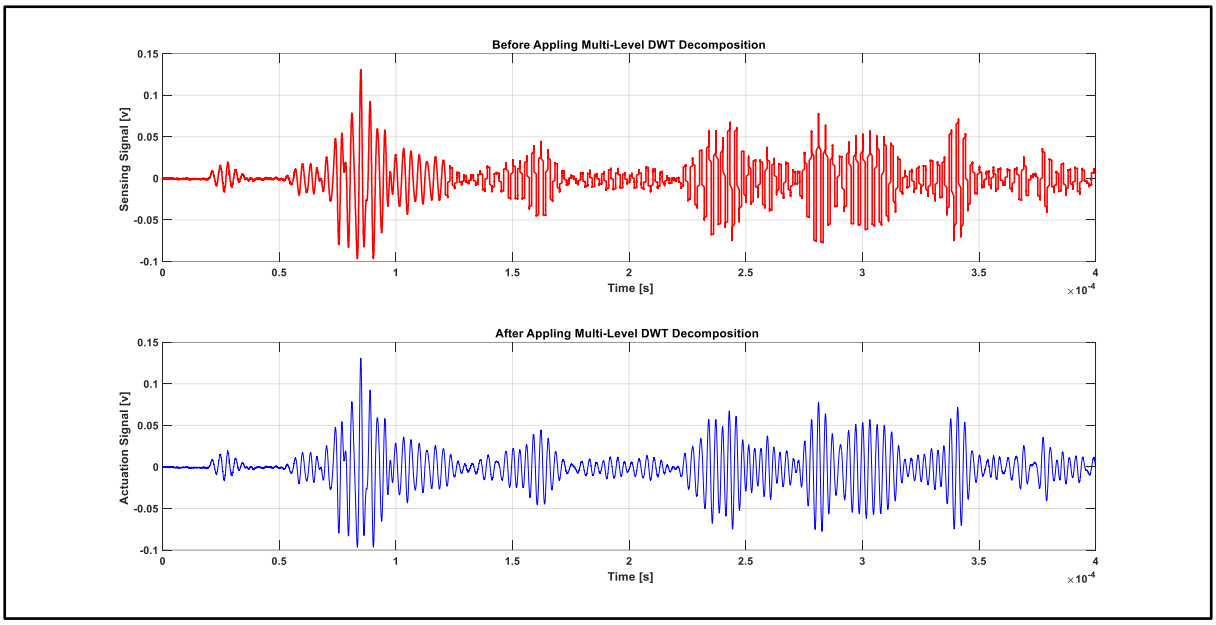

Figure 4. 1: Sensing signals before and after applying DWT.

4.3. Defect Location Algorithm

Detecting damage in the pressure vessel using ultrasonic inspection involves analyzing the ultrasonic signals for changes that may indicate the presence of defects or structural damage. However, the algorithm for defect location in the pressure vessel has been set to determine any changes on the pressure vessel, fig 4.2 shows the location algorithm.

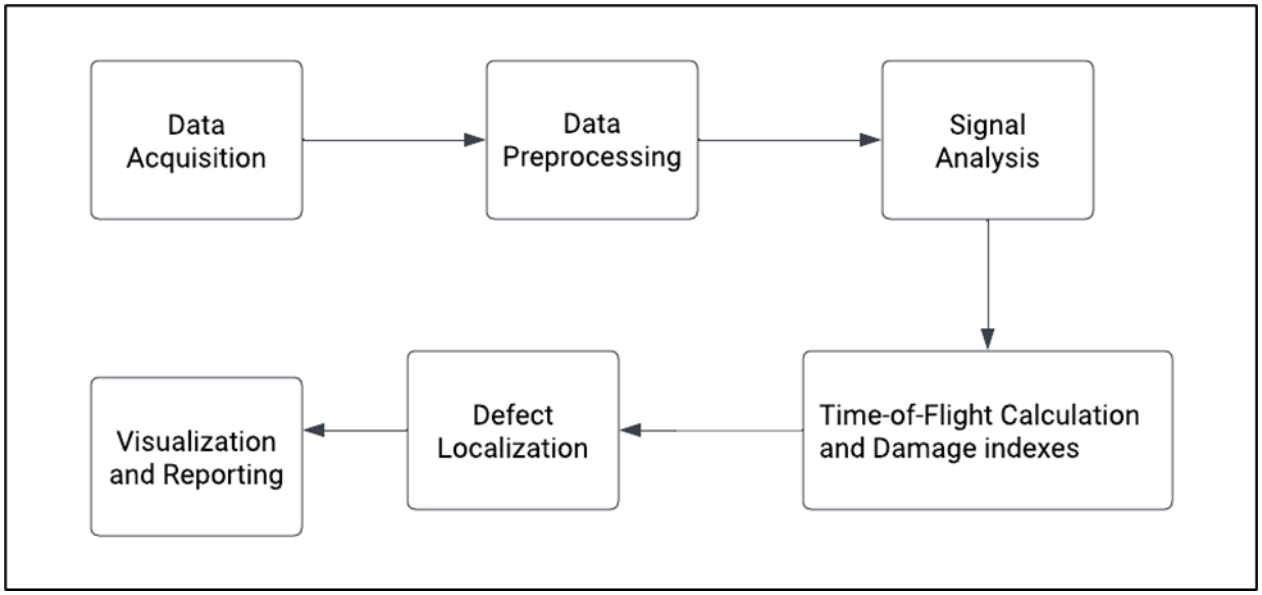

Figure 4. 2: Defect location algorithm for the pressure vessel

Data acquisition involves the utilization of ultrasonic transducers (PZTs) to emit ultrasonic waves into a water tank and subsequently gathering data from the PZT sensors in xlsx format. Following data acquisition, preprocessing is undertaken to enhance data quality, achieved through the application of Multi-level Discrete Wavelet Transform (DWT) to eliminate noise and sharpen the data for further analysis.

While signal analysis involves identifying and monitoring variations in modes, amplitude, and phase shift of signals. In addition to this, time-of-flight (ToF) calculations and damage indexes are crucial components of the process. ToF determines the time disparity between transmitted and received signals for each identified signal. Meanwhile, the Normalized Signal Energy (NSE) index detects alterations in signal amplitude, and the correlation coefficient deviation (CCD) identifies changes in signal phase shift. Lastly, the Root Mean Square Deviation (RMSD) provides insights into both amplitude and phase shift variations within the signal, facilitating a comprehensive analysis of signal characteristics. However, if any of these calculated values undergoes a significant change or exceeds certain limits, it indicates potential damage to the structure. By analyzing these values, the system can determine the location of the damage within the structure by building a 3D map of the structure.

Utilizing time-of-flight (ToF) measurements and the established speed of sound in water, defect localization becomes feasible by determining the distance to the defect. Analyzing the variations in damage index values across diverse sensor locations allows for accurate prediction of the defect's precise location. Subsequently, defect locations are visually represented and reported via an LCD screen, providing a thorough depiction of structural integrity essential for efficient monitoring, and reporting endeavors.

4.4. Summary and Conclusion

This chapter provides an in-depth discussion on damage indexes and signal smoothing, with a particular focus on establishing a defect location algorithm for pressure vessels. Various damage indexes, including RMSD, CCD, and NSE have been employed in this study. Some of these indexes, such as NSE, exhibit sensitivity to amplitude changes, while others, like CCD, are sensitive to phase shifts.

To address signal sharpness, a MATLAB implementation of a Discrete Wavelet Transform (DWT) filter has been utilized to smooth the sharp edges in sensing signals. However, the core of the defect location algorithm for pressure vessels is centered around identifying the Time of Flight (ToF) and damage indexes. A map is constructed based on the values of these indexes, and if a significant change or if the values exceed certain limits, it represents a sign that potential damage has occurred in the pressure vessel.

Chapter 5

5.1. The effect of changing the states on the ultrasonic inspection

Seven PZT transducers have been installed in the tank (2 actuators and 5 sensors). We keep the distance between the actuator and sensor less than 15 cm . The angle between the actuator and the sensors is 72^0. To enhance sensor response and ensure precise measurements such as S_0 and A_0, it is recommended to maintain a conservative distance of less than 15 cm between the actuator and all sensors.

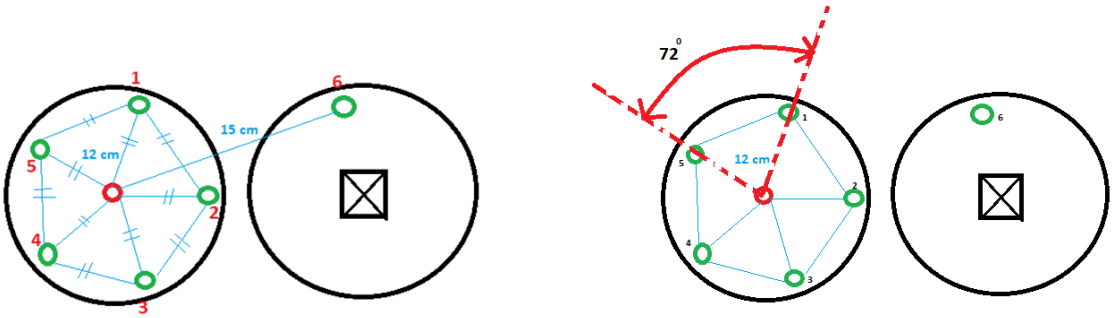

Figure 5. 1: The transducers location (the distance and the angle between them)

The actuation signal used is a 300kHz 5-peak Hann window applied to a location in the center of the tank structure (Figure 5.1). The input signal amplitude is 8.5Vpp using the max value of the waveform generator and no voltage amplifier connected to avoid concern in signal distortion. Four sensor signals were used in this experiment. The tank was initially tested in an empty state and then filled with water, the water temperature during testing was maintained at 22°C and no pressure effect.

The sensing signal in the empty and full tank conditions was compared graphically in Figure 5.2, A notable decline in signal arrival is observed after the initial wave packet in the full tank, and this pattern is consistent across all three sensing signals. The presence of the first wave packet arrival, representing the symmetric mode, remains, while the second wave packet, indicative of the antisymmetric mode, has diminished.

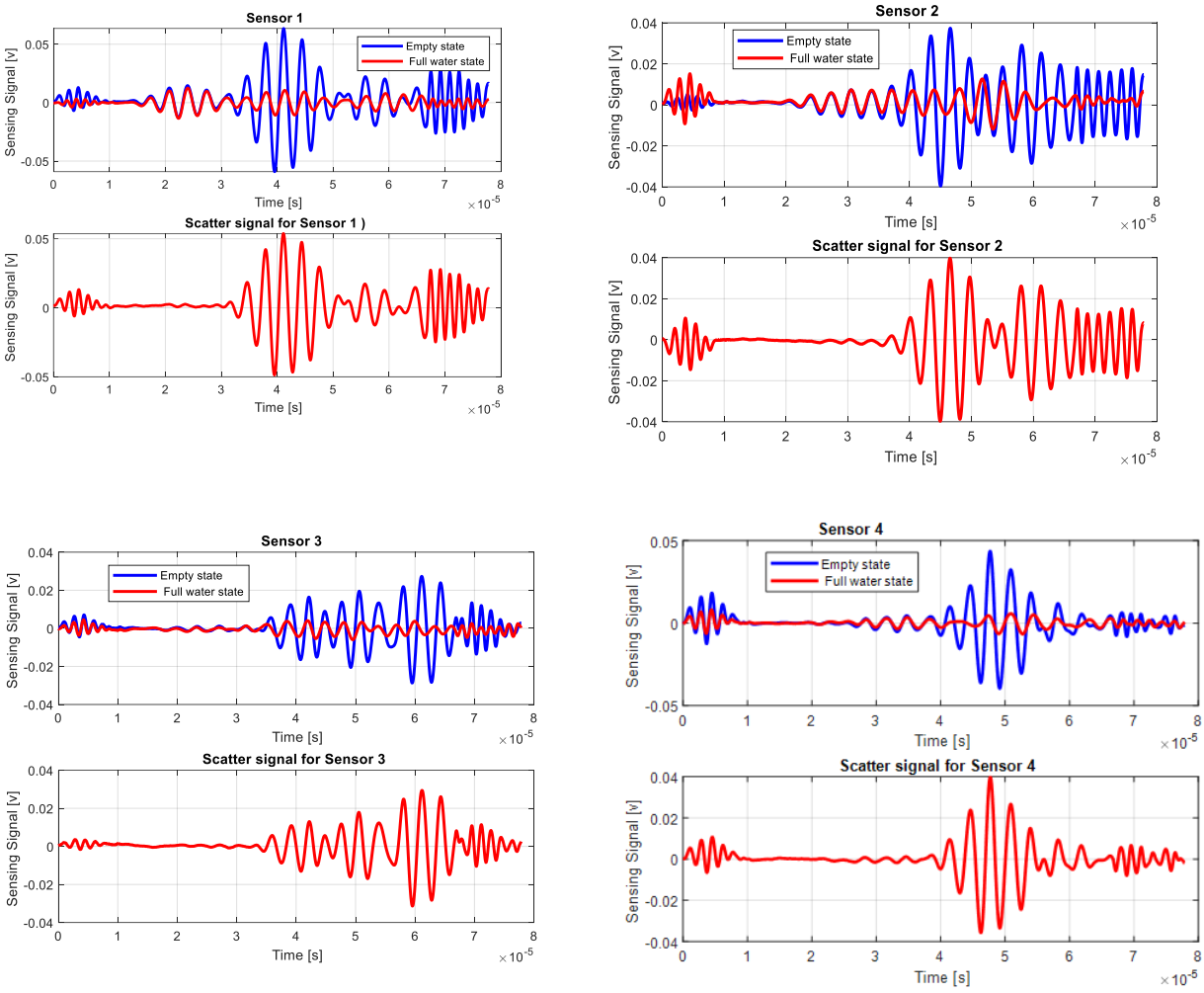

Figure 5. 2: Comparison between Full water state and Empty state for sensors response

Also, of note in Figure 5.2, there is no difference seen in the first wave packet arrival symmetric node signal characteristics (amplitude, ToF). The frequency domain for PZT transducers refers to the representation of its signals and responses in terms of frequency components rather than time [19]. In this domain, various frequencies present in the sensor's output can be analyzed, providing insights into its behavior across different frequency ranges. This analysis is particularly useful in understanding how a PZT sensor responds to specific frequencies and identifying any resonance or characteristic frequency patterns.

The RMSD, NSE, and CCD Damage indexes have been calculated by assuming the pristine state is the state of the structure, and the damage signal is when the state is full of water. However, the window time for the DI has been chosen to include the symmetrical (S_0) and unsymmetrical modes (A_o), figure 5.4 shows the Damage index time window for the first sensor.

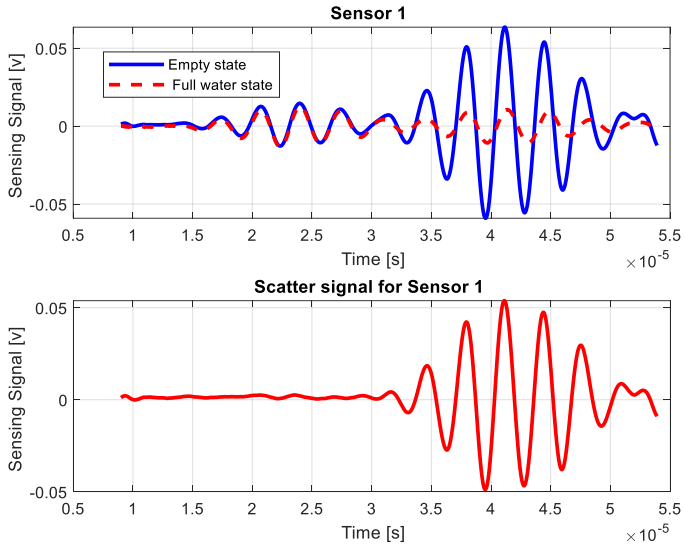

Figure 5. 3: Time window for the Damage index in the first sensor.

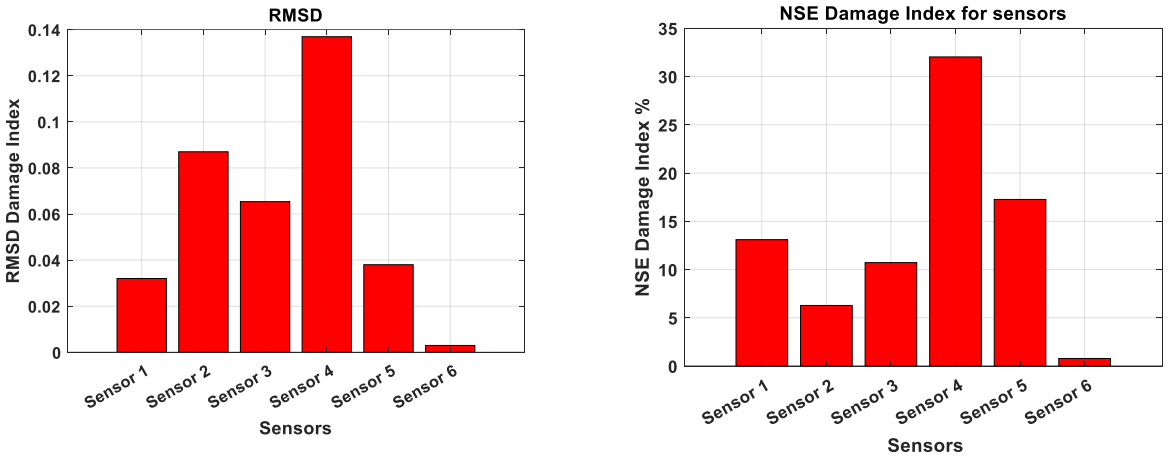

Figure 5. 4: RMSD and NSE damage indexes for empty and full states under 100 Psi pressure.

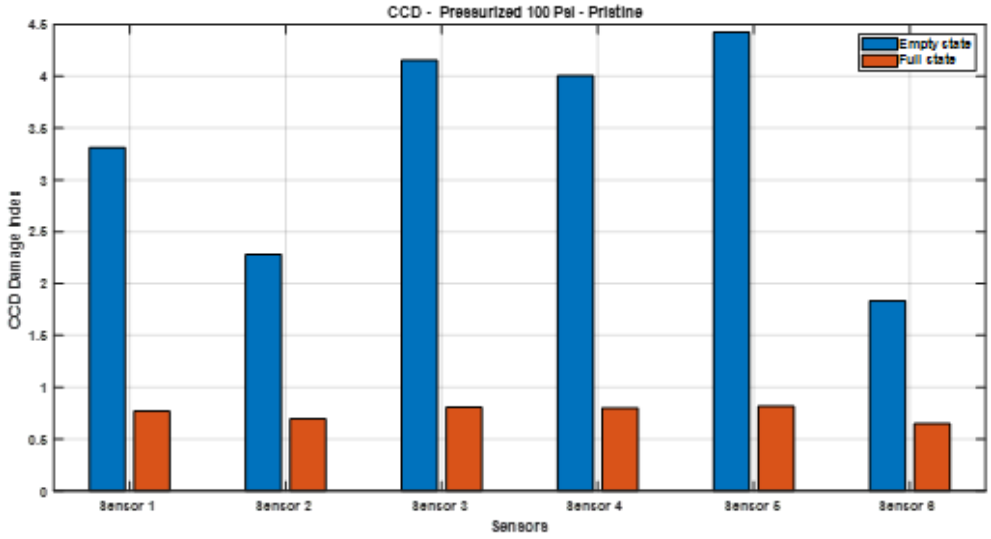

Figure 5. 5: CCD Damage index for the empty and full states under 100 Psi pressure.

The A_0 mode experiences a reduction and diminishes when the tank is filled with water, while the So mode remains unaffected in empty and full water states. However, identifying the locations of S_O and A_O for the sensors becomes easier, due to fixing the distance between the actuator and sensors less than 15 cm.

To evaluate the changes in the states, three damage index methods based on RMSD, CCD, and NSE were used to measure the difference between baseline signals (empty state) and the measured signals (full water state) over the first and the second wave packets. It is noteworthy that the CCD damage index is sensitive to both empty and full states, as evidenced by consistently higher values in the empty state compared to the full state. RMSD and CCD show sensitivity to state changes caused by wave attenuation. This sensitivity arises from the gradual decrease in the magnitude of the second wave packets and is also influenced by structural complexity, such as rounded edges and holes in the structure. (figs 5.4 and 5.5) show the damage indexes.

5.2. The response of sensing signals to simulated damage.

The key component of this work is to build a physics-based ultrasonic inspection to find and localize the degradation and the defects on the pressure vessel. Therefore, simulated damage such as (Magnets, and sticky patches) has been used to validate the structural sensitivity of the damage. To do that we need to look for any changes in the signal such as changes in signal attenuation, time of flight, phase shift, alignment of the waveform in the group packet, signal energy, frequency content (Fourier transform)

5.2.1. Empty state

Sticky patches have been chosen as temporary simulated damage on the pressure vessel, The sticky material may introduce damping effects on the PZT sensor and add new mass to the structure, which can affect the sensor's sensitivity and resonant frequency. However, the empty tank without sticky patches has established a baseline measurement while the empty tank with sticky patches has established simulated damage, any deviation from this baseline can be flagged as a potential issue. The sticky patch has been mounted around the sensor one as shown in fig 5.6.

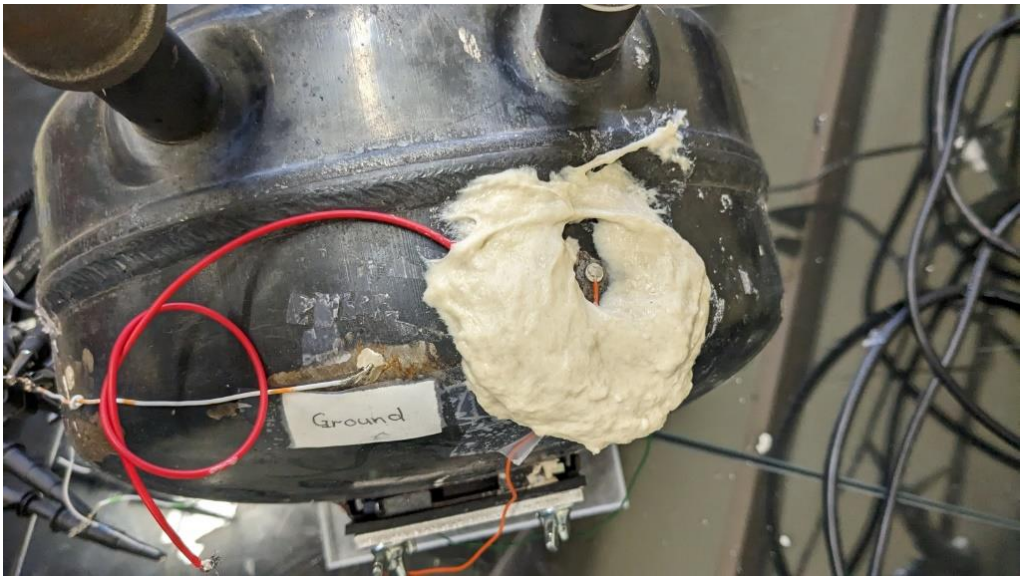

Figure 5. 6: picture for the sticky patches mounted around sensor 1

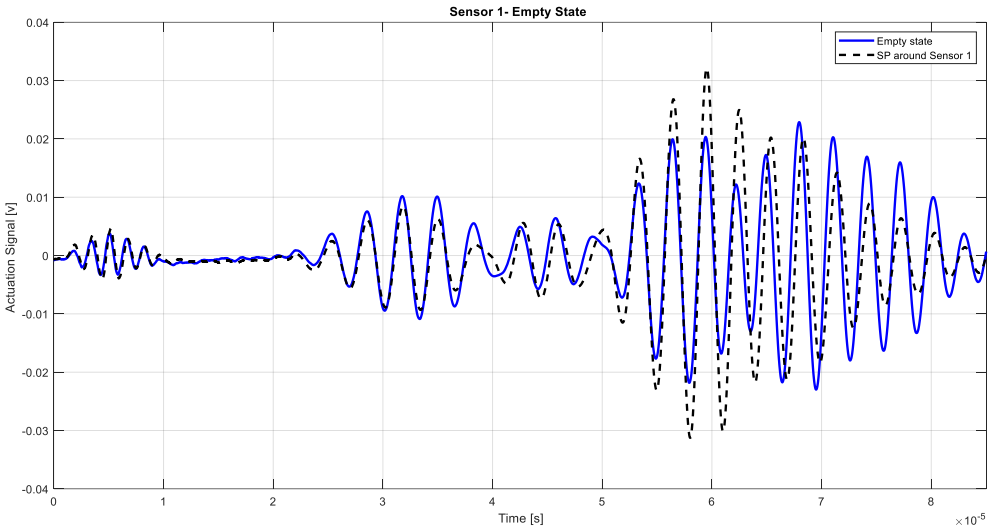

Figure 5. 7: Effect of sticky patches on the sensing signal for the empty state.

Based on fig 5.7, it is evident that simulated damage notably influences the asymmetrical mode Ao of the sensor response, as indicated by the amplified amplitude of Ao. Conversely, the amplitude of So exhibits minimal variation. To validate this observation, an alternative simulated damage scenario involving Neodymium Magmatic was employed. The comparison depicted in the fig 5.8 illustrates the difference in sensor response between the absence and presence of magnetic material around sensor 1, Subsequently, the results affirm that simulated damage, whether in the form of sticky patches or magnetic effects, exerts a notable influence on the Ao mode.

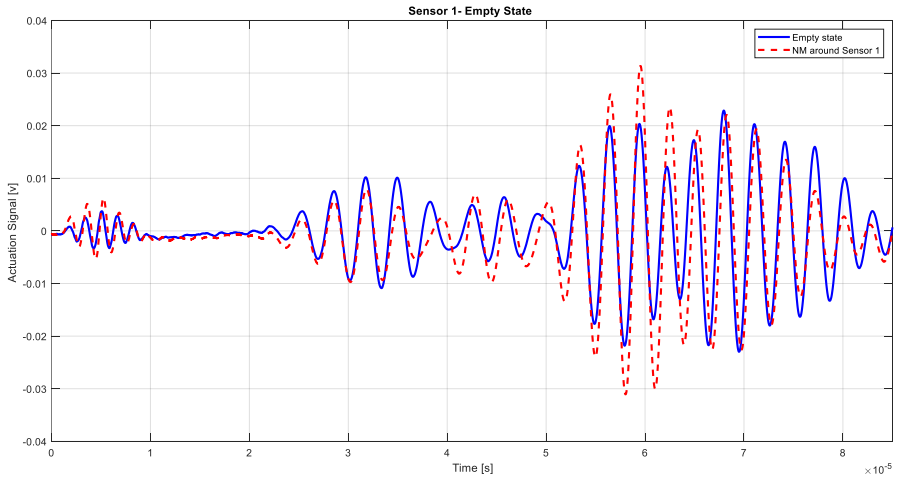

Figure 5. 8: Effect of Neodymium magnetics on the sensing signal for the empty state.

5.2.2. Full water tank

The study continues to investigate the behavior of a pressure vessel full of water under ambient pressure and at room temperature conditions. Simulated damage, in the form of both sticky patches and magnetic effects, is employed to verify the response signal. However, any deviation observed from this established baseline is indicative of potential structural damage in the vessel. To make sure that the water during testing has been maintained at 22°C, we store the water in a large container for approximately 30 minutes. Subsequently, the water was transferred into the test tank, and its temperature was confirmed using a thermometer. The pressure within the tank was regulated to match ambient pressure by fully opening the water valve during experimentation.

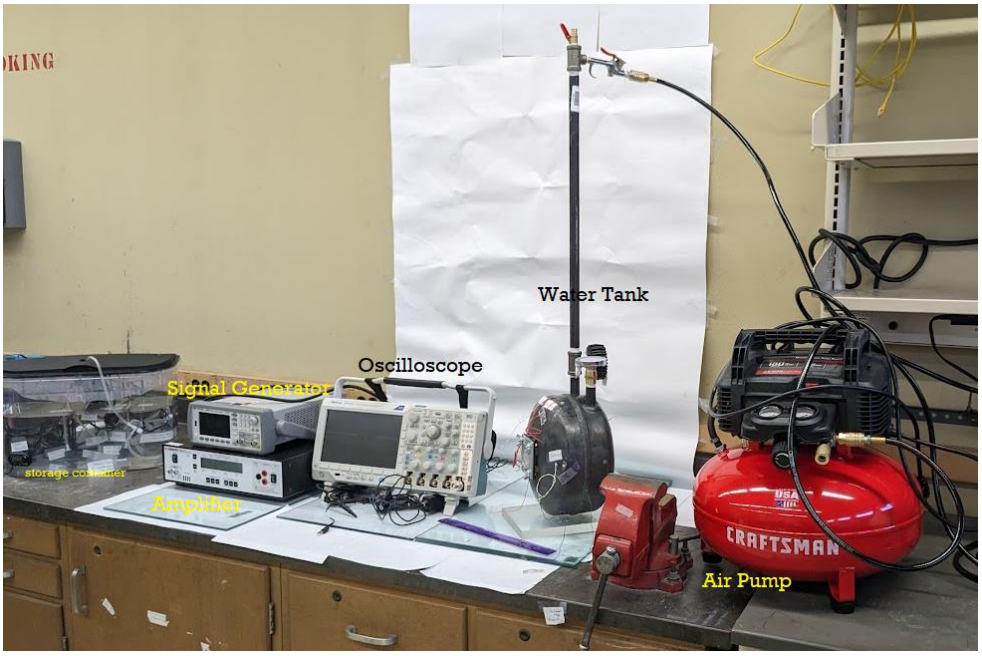

Figure 5. 9: Experimental setup for the pressure vessel

The experimental setup depicted in fig 5.9 which contains a storage water container for maintaining water temperature at 22°C, along with a signal generator, amplifier, oscilloscope, and the water tank (pressure vessel). The utilization of an air pump for testing the tank under static pressure will be studied in the next chapter. Moreover, a thermometer

and pressure gauge are attached to the tank to measure both water temperature and static pressure.

Fig 5.10 and 5.11 illustrate a comparison between the pristine state (full water) and the simulated damage state (with sticky patches and Neodymium magnets). In the full water state, the Ao mode is diminished, as discussed earlier. However, when simulated damage is introduced to the tank, the Ao mode becomes even weaker, while the So mode experiences a slight change in the amplitude. However, a slight angle shift Ao has been observed between the two signals, indicating the presence of simulated damage.

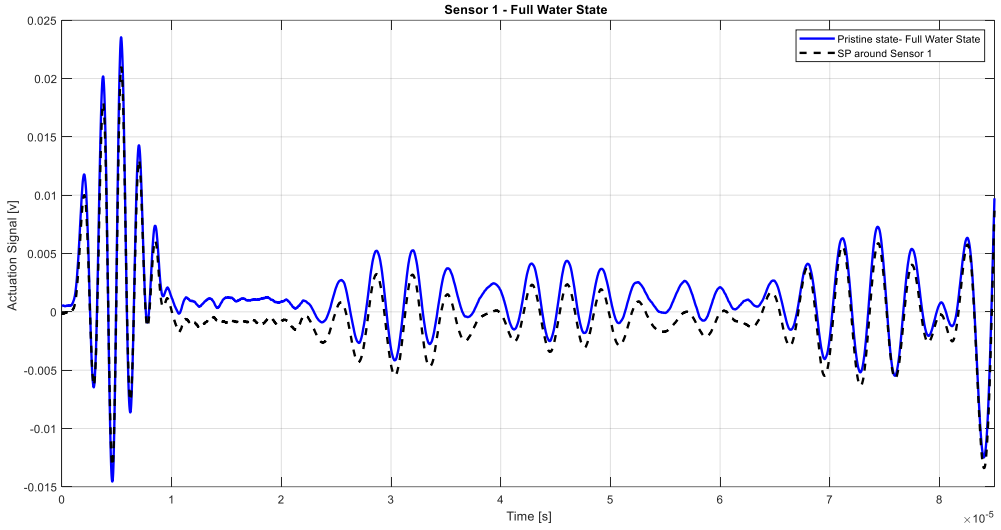

Figure 5. 10: Effect of the sticky patches on the sensing signal at full water state

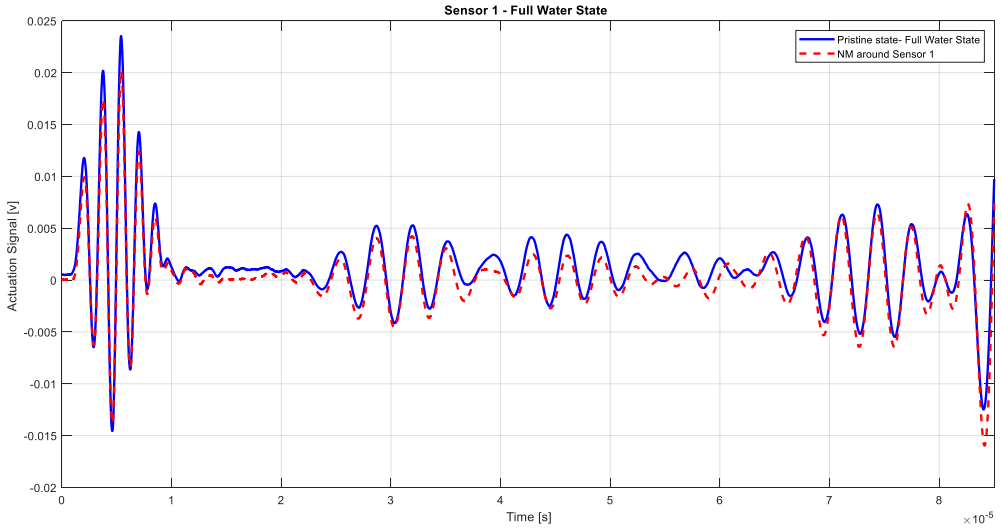

Figure 5. 11: Effect of the Neodymium magnetics on the sensing signal at full water state

5.3. Summary and Conclusion:

Chapter 5 explores the impact of changing states, specifically comparing an empty tank to one filled with water, on ultrasonic inspection using PZT transducers. Seven transducers are installed in the tank, with distances between the actuator and sensors maintained for optimal performance and good sensor response. A 300kHz 5-peak Hann window actuation signal is applied, with signal characteristics documented for both empty and filled tank conditions. In the filled tank scenario, a decline and diminish in second packet arrival signals (A_0) has been observed across all sensing signals in the full water state.

Three damage index methods, namely RMSD, CCD, and NSE, were utilized to assess changes in states by comparing baseline signals (empty tank) to measured signals (tank filled with water) over the first and second wave packets. Notably, the CCD index demonstrated sensitivity to both empty and full states, with consistently higher values in the empty state. RMSD and CCD were sensitive to state changes due to wave attenuation, attributed to the gradual decrease in the magnitude of the second wave packets, structural complexity, such as rounded edges and holes, also influenced sensitivity.

The pressure vessel was also examined under simulated damage (Sticky patches and Neodymium magnets) under controlling environmental conditions. In the empty state, the simulated damage significantly affects the asymmetrical mode (A_0) of sensor response, with amplified amplitude while the amplitude of the symmetrical mode (S_0) shows minimal variation. On the other hand, when the pressure vessel is in the full water state, the A_0 mode is already diminished, as previously discussed. However, with the introduction of simulated damage to the tank, the A_0 mode weakens further, while the So mode shows slight changes in amplitude. Additionally, a slight angle shift in A_0 between the two signals is observed, indicating the presence of simulated damage.

Chapter 6:

6.1. Investigating the Impact of Pressure on Ultrasonic Inspection for the pressure vessel.

Theis chapter focuses on assessing how variations in pressure affect the efficacy of ultrasonic inspection techniques specifically for pressure vessels. This work aims to understand how changes in pressure influence signal propagation through the structure and the ability of ultrasonic techniques to detect potential defects and cracks, within the pressure vessel's material.

6.1.1. Studying the pressure effect without any simulated damage

Through studying the pressure effects without introducing simulated damage, we can establish a baseline understanding of how pressure alone impacts ultrasonic signals, which provides a fundamental understanding of how pressure influences signal propagation, attenuation before introducing the damage.

6.1.1.1 Empty state

The pressure vessel was tested initially under atmospheric pressure conditions and then pressurized the vessel to an internal pressure of 100 (Psi). This pressurization was facilitated using an air pump to reach the desired 100 Psi target pressure. A pressure gauge was employed throughout the process to monitor and ensure that the internal pressure reached the specified 100 Psi level accurately, Next, a one-minute waiting to allow the system to stabilize, ensuring a steady state—subsequently, the ultrasonic inspection by activating the actuator on the PZTs and recording the corresponding sensing signals. Both signals (under atmospheric pressure and 100 Psi) have been compared and extracted the main differences features in the sensor's response.

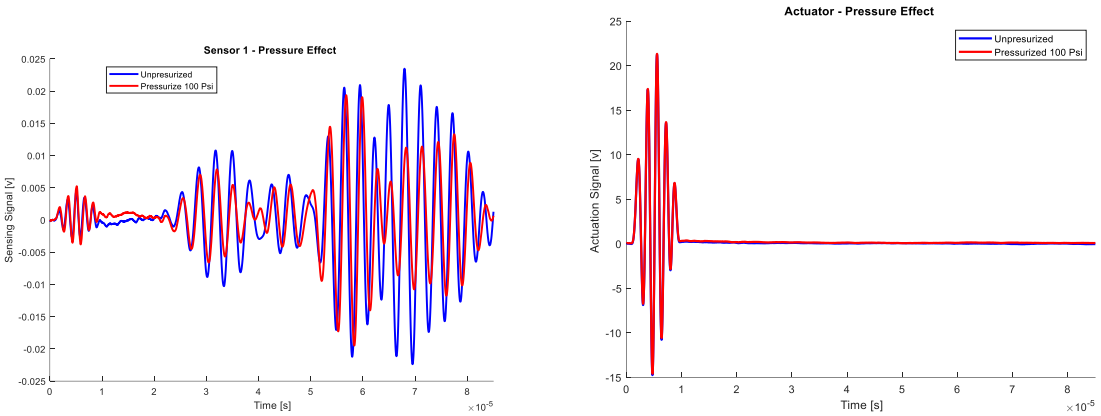

Figure 6. 1The pressure effect for the sensing and the actuation signals at the empty state.

Fig 6.1 shows how the pressure affects the sensing signal in the pressure vessel and how the pressure impacts both the first and the second packets' arrival. However, the figure shows a significant decrease in the symmetrical mode S_0, while only a slight decrease is apparent in the asymmetrical mode A_0. Moreover, a minor distortion is observed at the end of the first packet arrival.

6.1.1.2. Full water state

The identical procedures and settings used in the empty state were replicated in the full water state, with the water temperature maintained at 22°C. However, the sensing signal was plotted at both ambient pressure and 100 Psi in the fig 6.2 . It is evident that pressure influences the asymmetrical mode, reducing its amplitude, while the symmetrical mode S remains unaffected by pressure.

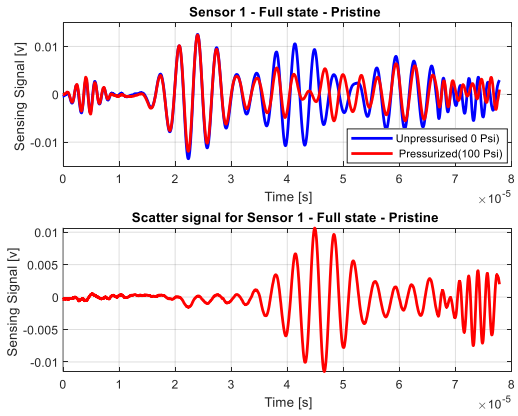

Figure 6. 2: The effect of the pressure in the sensing and actuation signal at full state

6.2. Studying the pressure effect with simulated damage:

Sticky patches and neodymium magmatic elements were utilized to address structural damage. The tank was subjected to testing in both empty and full water states under 100 Psi pressure. Simulated damage was placed around sensor 1.

6.2.1. Empty state

An investigation was conducted to assess the effects of simulated damage on a tank pressurized to 100 Psi. As a result, adhesive patches were placed around sensor 1. Fig 6.3 illustrates the comparison between signals with and without these patches. Both signals showed decreased amplitude at S_0 and distortion following the first packet arrival, as outlined in section (6.1.1.1). However, introducing adhesive patches around sensor 1 revealed a slight increase in the first and second arrivals packets during simulated damage, as observed from the scatter signal.

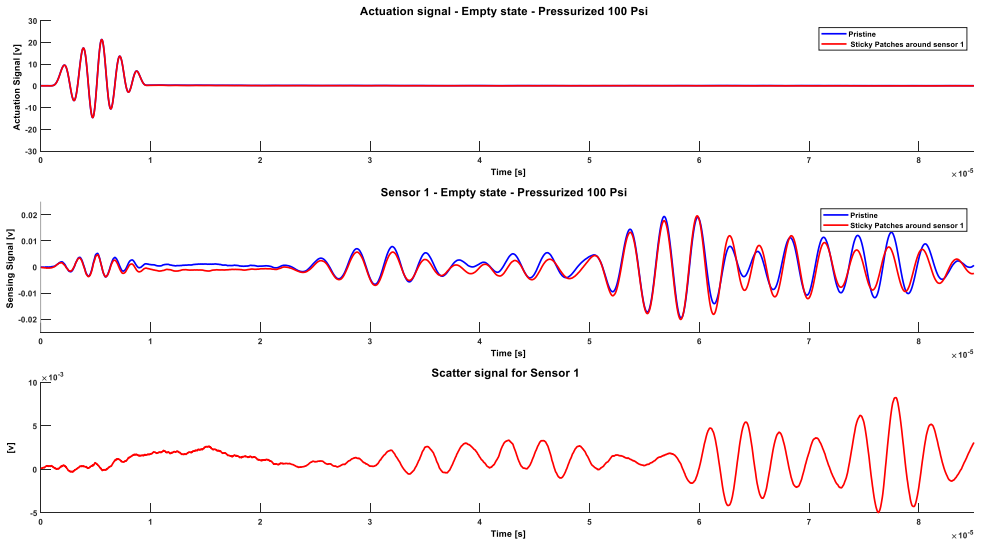

Figure 6. 3: The effect of the simulated damage in the actuation signals, sensing signal and the scatter signal for the empty state under 100 Psi.

6.2.2. Full water state

In the case of the tank being filled to its full water capacity at 100 Psi pressure, we observe that the second arrival of the A_0 packet diminishes due to propagation through water

and experiences a reduction in amplitude owing to pressure effects. Nonetheless, the introduction of simulated damage also has a minor impact on the A_0 signal, resulting in an increase in amplitude, as depicted in fig 6.4. The second arrival packets are significantly disrupted as the signals traverse through water, making it challenging to investigate the effects of simulated damage on the structure. However, in the empty state, it becomes distinctly evident how simulated damage affects the second packet's arrival.

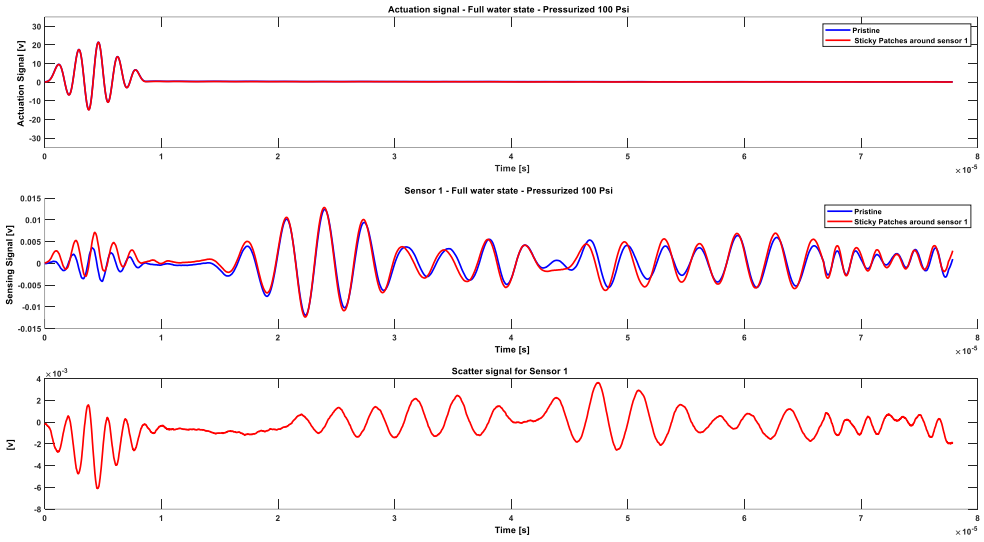

Figure 6. 4: The effect of the simulated damage in the actuation signals, sensing signal and the scatter signal for the full state under 100 Psi.

6.3. Damage index calculation:

In structural health monitoring (SHM), damage indexes play a crucial role in measuring differences between signals and predicting damage locations by examining changes in these indexes. This section utilizes various DI techniques including RMSD, CCD, and NSE to evaluate the effects of simulated damage in full water conditions at 100 Psi. The structure is subjected to testing both with and without simulated damage, and DI calculations are performed for each sensor. The evaluation of the DI involved by introducing simulated damage at specific locations within the structure, each directly obstructing the actuation signal to at least three sensors, either partially or completely. The sensor response and the DI

have been studied deeply to figure out the effect of the sticky patches in the structure. The time window for the DI calculation has included the first and the second packets arrival.

6.3.1. The sticky patch is located on the first tri-sector of the tank.

A large sticky patch covers the area spanning from the actuator to sensors 1, 2, and 3, as depicted in fig 6.5 . The responses of these sensors have been recorded and analyzed in fig 6.6.

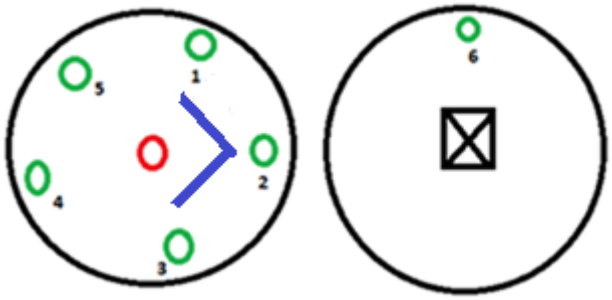

Figure 6. 5: The location of the simulated damage in the structure between the actuator and sensors 1,2 and 3.

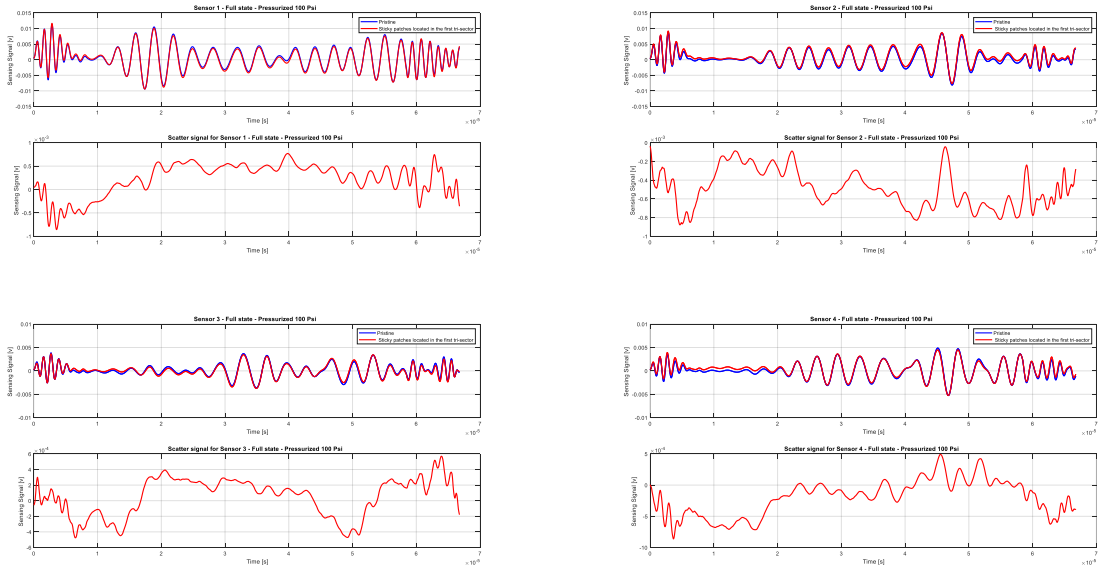

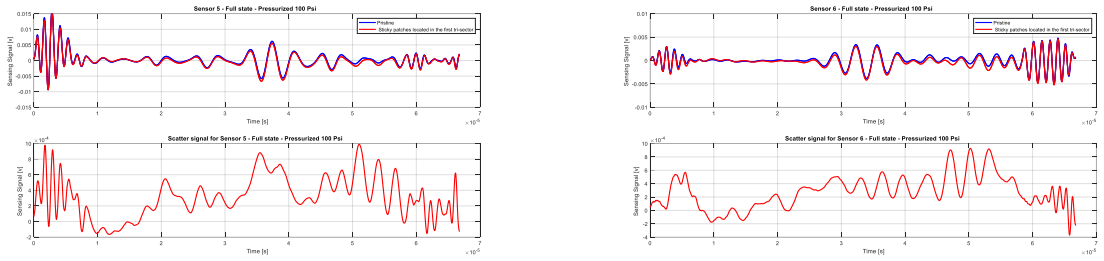

Figure 6. 6: The effect of the simulated damage on the sensing signal for six sensors and there scatter for Full state under 100 Psi

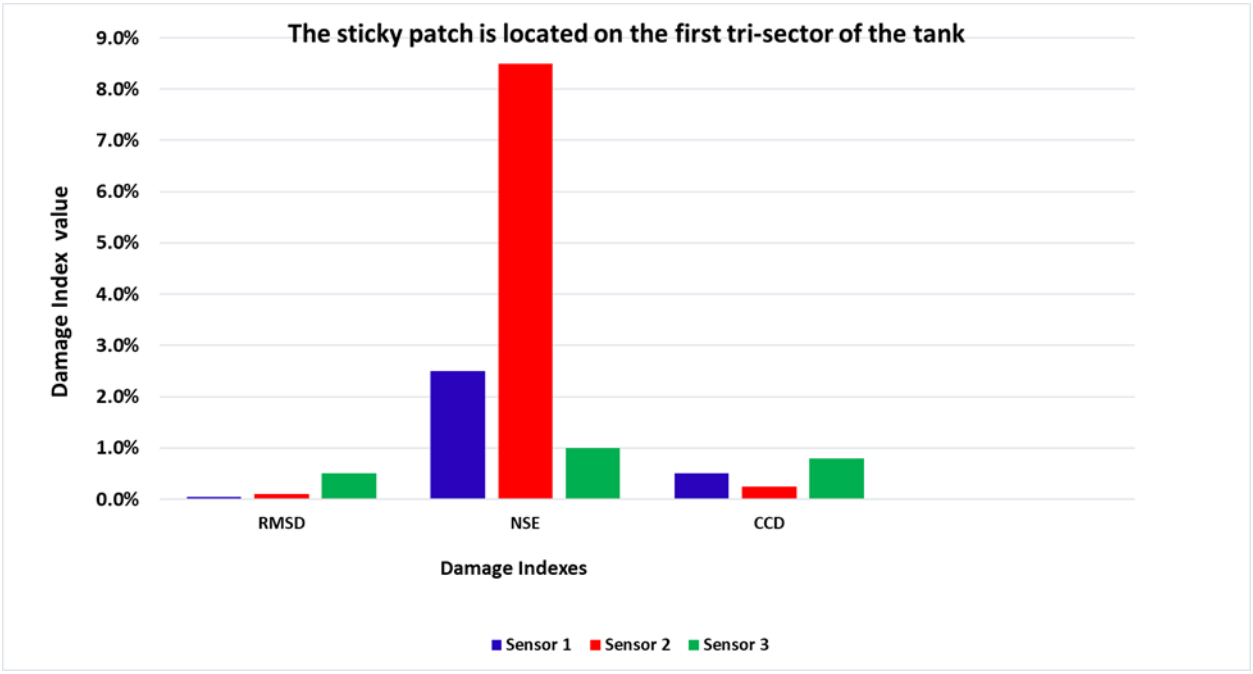

Figure 6. 7: the values of damage index methods (RMSD, NSE, and CCD) for sensors 1,2 and 3.

Observing fig 6.7, it's evident that the NSE damage index exhibits a notably higher value in contrast to RMSD and CCD. Previous studies indicate NSE's sensitivity to signal attenuation, which we point out in section 6.2.2. Specifically, we demonstrate that the second arrival packet (A_0) displays heightened sensitivity to simulated damage by amplifying its amplitude compared to the first arrival packet (S_0). Furthermore, it's apparent that sensor two records a significant NSE value. This is due to simulated damage completely obstructing all actuation signals. In contrast, sensors one and three only partially block the actuation signal.

6.3.2. The sticky patches are located on the second tri-sector of the tank.

To validate the findings concerning the sensitivity of NSE to simulated damage, we placed the simulated damage in the second sector of the tank. However, the actuation signal has completely obstructed sensor 3 and partially influenced sensors 2 and 4, as depicted in the provided fig 6.8.

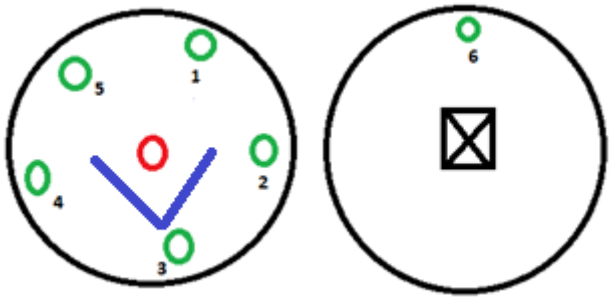

Figure 6. 8: The location of the simulated damage in the structure between the actuator and sensors 2,3 and 4.

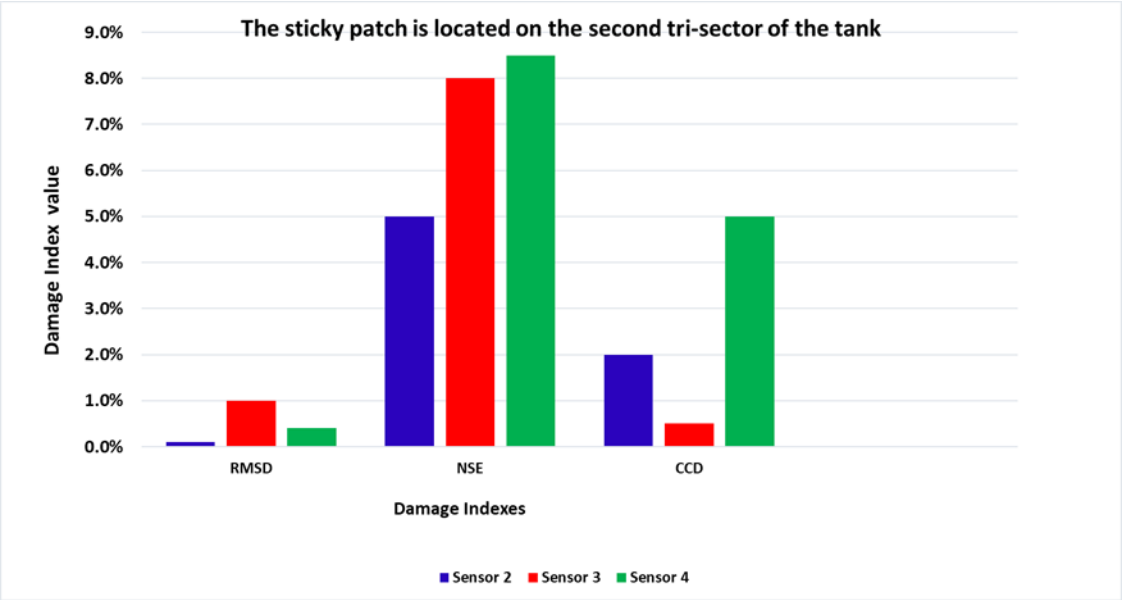

Figure 6. 9: the values of damage index techniques (RMSD, NSE, and CCD) for sensors 2,3 and 4.

The NSE damage index exhibits a significant value compared to other indexing methods. Notably, sensors 3 and 4 show the highest NSE values, indicating that the simulated damage affects these sensors to a greater extent. In contrast, sensor 2 exhibits the lowest NSE value.

6.3.3. The sticky patches are located on the third tri-sector of the tank.

To confirm the results about the sensitivity of NSE to the simulated damage, we put the simulated damage in the third sector of the tank, which obstructed sensor 5 and partially sensors 3 and 4 as shown in fig 6.10.

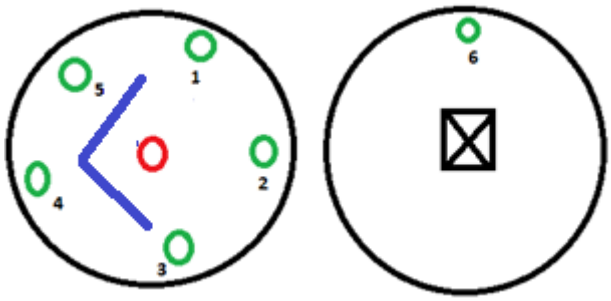

Figure 6. 10: The location of the simulated damage in the structure between the actuator and sensors 3,4 and 5.

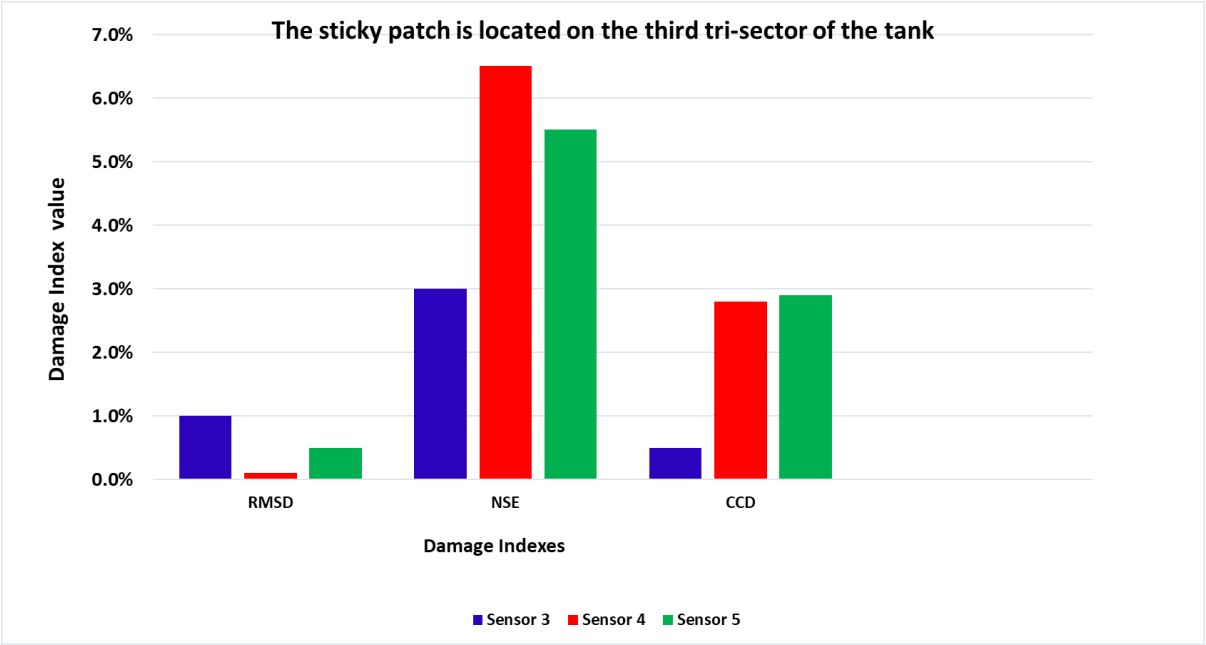

Figure 6. 11: the values of damage index techniques (RMSD, NSE, and CCD) for sensors 3,4 and 5.

The results confirm that NSE showed a higher value in comparison to RMSD and CCD. Sensor four recorded a higher value due to complete obstruction of the actuation signals, whereas sensors three and five faced partial obstruction. Moreover, the experiment was replicated with adhesive patches positioned on the opposite side of the tank, as depicted

in the fig 6.12, sensor five was entirely obstructed from the actuation signal, while sensors four and one experienced partial obstruction. Fig 6.13 demonstrates that sensor five displayed the highest NSE damage index among other sensors and different damage index methods.

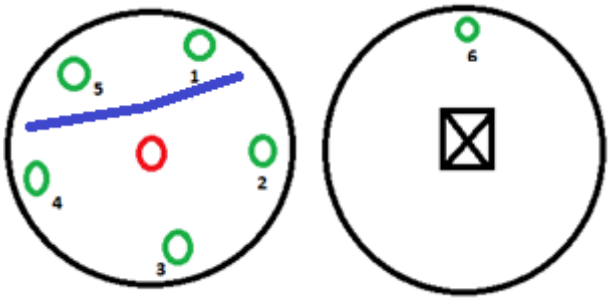

Figure 6. 12: The location of the simulated damage in the structure between the actuator and sensors 5,6 and 1.

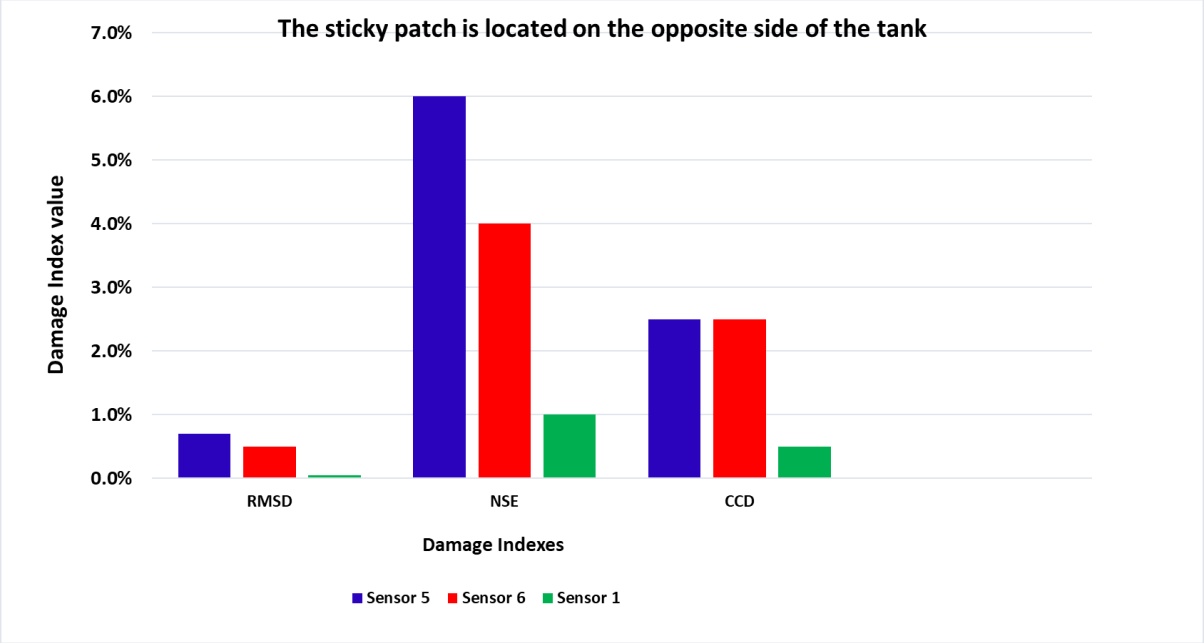

Figure 6. 13: the values of damage index techniques (RMSD, NSE, and CCD) for sensors 5,6 and 1.

In summary, the impact of simulated damage at various locations on the pressure vessel has been assessed using different methods for calculating damage indexes. These indexes have been graphed individually for clarity. Most of the values of the RMSD damage index are too low (less than 2%). Therefore, there is a big challenge to identify the damage location exactly based on the RMSD DI, while the NSE can sense that there are sticky

patches on the structure, and it can predict exactly the location of the sticky patches. On the other hand, most of the values of the CCD damage index are less than 3%. Therefore, there is a big challenge to identify the damage location exactly based on the CCD damage index. Fig 6.14 shows the RMSD, NSE and CCD damage index at different sensors and locations of the simulated damage.

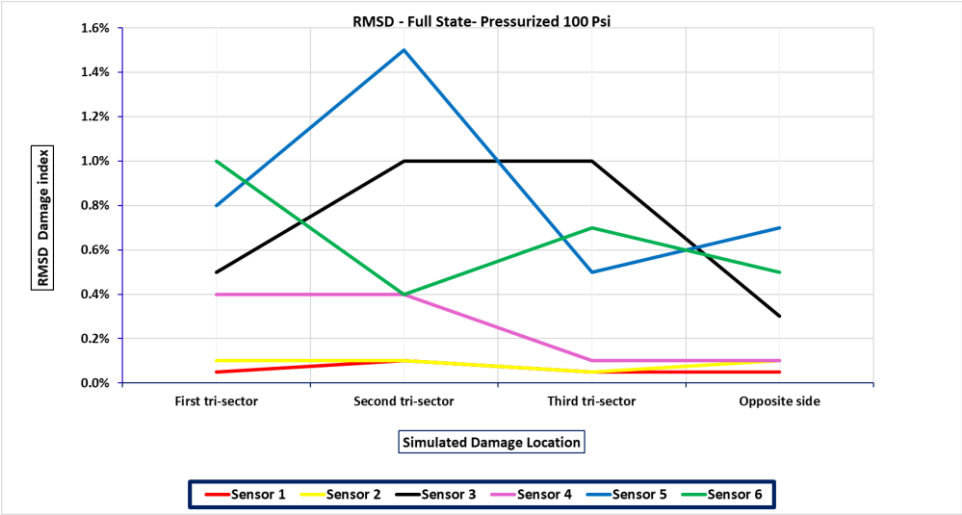

a)

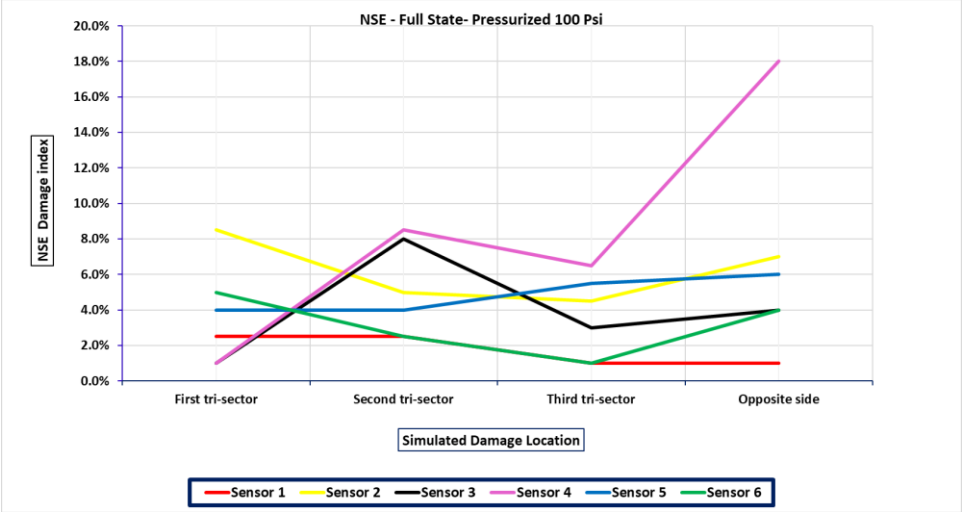

b)

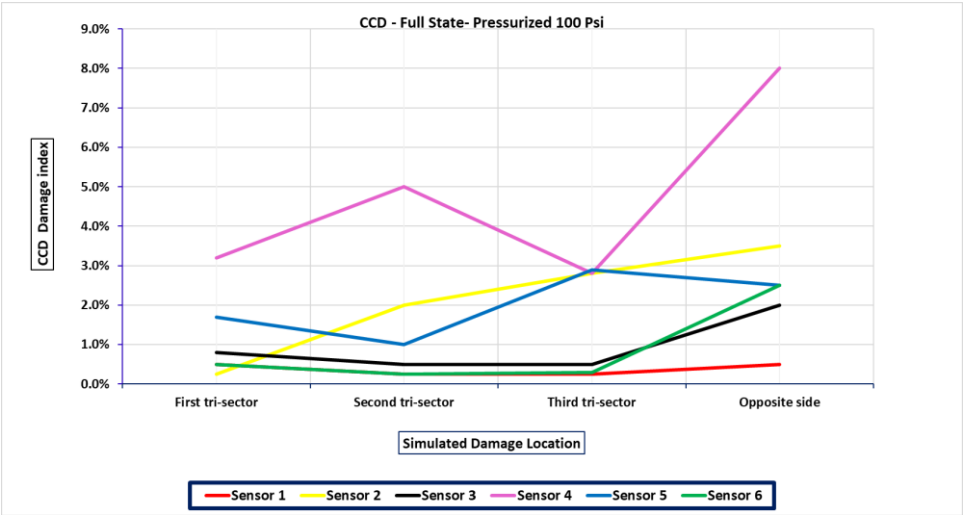

c)

Figure 6. 14: a) values of RMSD for all sensors at different damage location, b) values of NSE for all sensors at different damage location, c) values of CCD for all sensors at different damage location

6.4. Summary and Conclusion

This chapter into building physics understanding base for the influence of pressure on ultrasonic wave propagation within pressure vessels, whether empty or filled with water. We observe that in an empty tank, the pressure significantly reduces the amplitude of symmetrical mode S_0 and slightly affects asymmetrical mode A_0 amplitude. Conversely, in a water-filled tank, the pressure primarily affects antisymmetric mode by reducing its amplitude, while symmetrical mode S_0 remains unchanged.

The study then examined the impact of simulated damage along with pressure on both empty and full water tanks by introducing adhesive patches around sensor 1. Results showed a slight decrease in the first and second arrival packets due to simulated damage when the tank was empty, also the results revealed a minor impact on the A_0 signal by decreasing the amplitude when the tank was full of water. Therefore, the simulated damage had a minor impact on the second arrival packet in both states. However, as previously discussed, the signal propagation of the second arrival packets was disrupted by water traversal and experienced energy loss due to pressure effects, which made the investigation of simulated damage effects on the structure challenging, especially in a full water tank. Conversely, in an

empty tank, the influence of simulated damage on the second packet's arrival is clear, because the second arrival packet preserved it is shaped and did not diminish in the empty state.

In the final section of this chapter, our focus was on the exploration and utilization of various Damage Index (DI) techniques, namely RMSD, CCD, and NSE, to assess the impact of simulated damage under full water conditions at 100 Psi. This evaluation involved introducing simulated damage at specific locations within the structure, each directly obstructing the actuation signal to at least three sensors, either partially or completely. The results indicate that the NSE method demonstrates greater sensitivity in detecting simulated damage compared to RMSD and CCD. Additionally, the NSE method enables us to identify which sensors experience complete obstruction of the actuation signal. In contrast, RMSD and CCD exhibit lower sensitivity to simulated damage due to their lower values.

Chapter 7:

Damage localization algorithm.

This chapter concentrates on developing an algorithm to detect and localize damage in a pressurized vessel operating at full water state with a pressure of 100 Psi. The algorithm utilizes both the first and second arrival packets. Furthermore, the research explores the optimal number of transducers **required** to cover the structure effectively.

7.1. The optimal number of transducers.

In section 5.1, we discussed the advantages of maintaining less than 15 cm between the sensors and the actuator to ensure optimal sensor response and to preserve the shape of So and Ao without distortion. Therefore, we decided on a conservative approach and maintain 12 cm between the actuator and sensors. Therefore, we distributed five PZT across the structure, with an angle of 72° between each of them.

We assume the tank has cylindrical shape with a diameter (D) of 0.25 m and a height (h) of 0.1 m. Consequently, the total surface area of the tank is calculated to be 0.1767 m^2. However, each sensor can cover a circular area with a diameter of 0.24 m, equal to 0.0452 m^2. Therefore, to determine the minimum number of PZTs required to cover the structure, we divide the total surface area of the tank by the area covered by one sensor. This yields a requirement of at least 4 sensors to cover the entire structure, totaling 5 transducers (one actuator and four sensors).

The 2-D representation illustrating the sensor coverage has been shown in the fig 7.1 the blue circle represents the total area of the structure surface (diameter = 0.474 m), while the red circle represents the coverage of the total area of one PZT as an actuator (diameter = 0.24 m), and the four black circles represent the coverage of the 4 sensors.

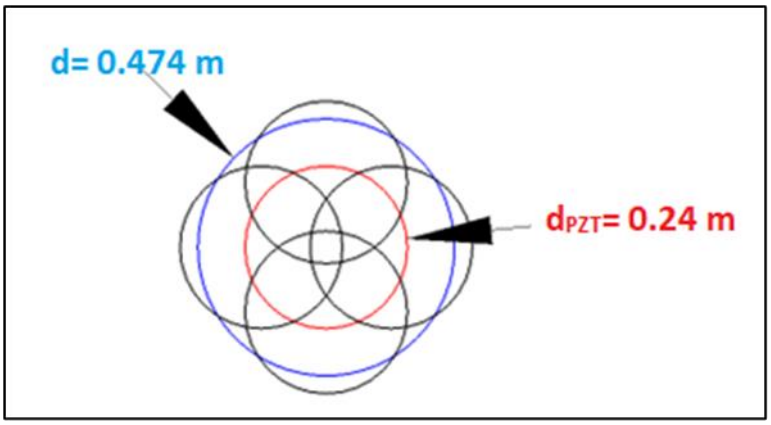

Figure 7. 1: 2-D representation of the coverages for the PZTs sensor

If simulated damage happens within an area where the coverage of multiple sensors overlaps, the precision of detecting and pinpointing the damage improves, as illustrated in fig 7.2. Conversely, if the damage occurs within a region covered by just one sensor, detecting and locating the damage becomes challenging, as depicted in the figure.

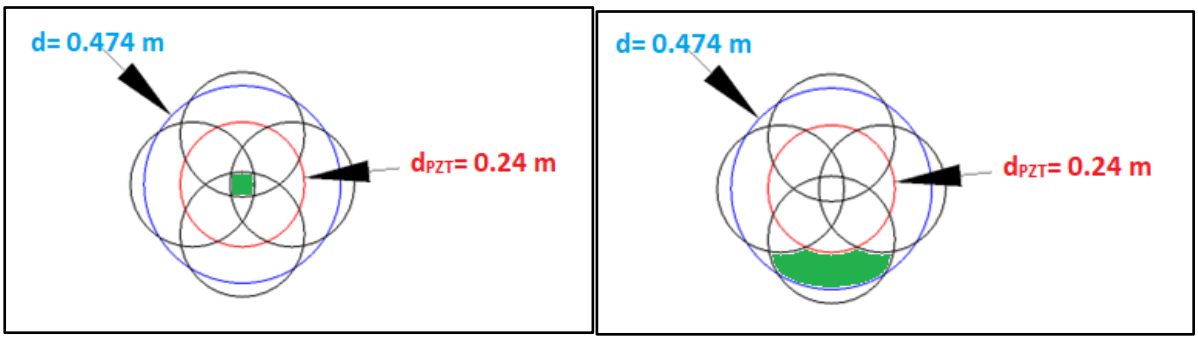

Figure 7. 2: 2-D representation of the overlap and non-overlap regions covered by the sensor coverage.

Certain regions on the structure as shown in fig 7.3 have a lack coverage (highlighted in red), but this deficiency can be compensated for by extending coverage to areas outside the structure (highlighted in green). However, increasing the number of transducers beyond five would enhance the structure's capability to detect damage.

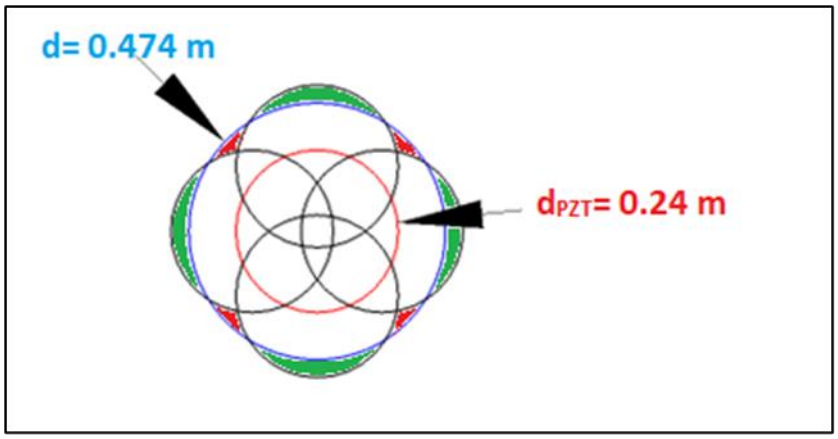

Figure 7. 3: Insufficient coverage (highlighted in red) and areas extending beyond the structure (highlighted in green).

The 3-D graphic representation was used for more accuracy based on that we find that we need 7 transducers (5 sensors and 2 actuators) to keep the distance between transducers around 12 cm and the angle between them being 72°. The two actuators have been placed in the middle of the tank (one actuator for each face) and the 5 sensors have been placed in a circle pattern with an angle of 72° and 12 cm from each actuator, the fig 7.4 shows the PZTs the green color are the sensors, and the red are the two actuators).

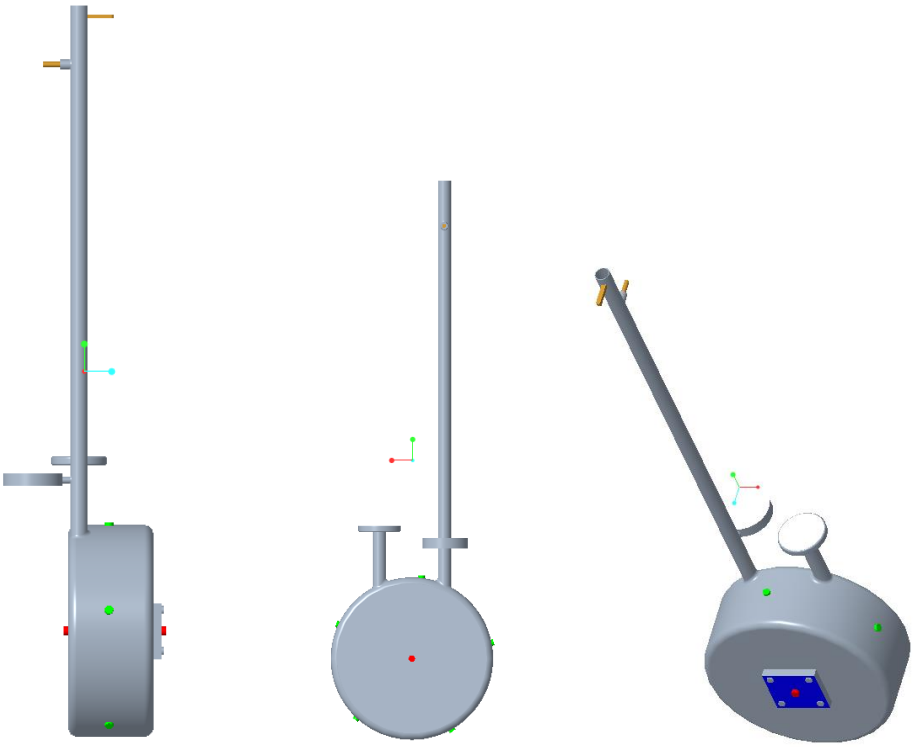

Figure 7. 4: the 3-D representation for the coverages for the PZTs sensor in 2

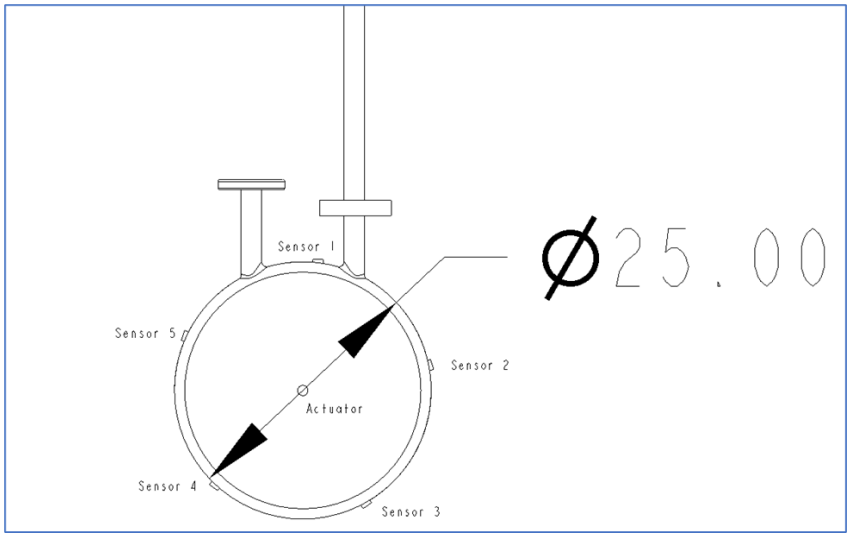

Figure 7. 5 : Dimension of the pressure vessel with sensors locations.

7.2 Damage localization algorithm based on the ToF.

The damage location can be determined using either S_0 reflection or A_0 reflection. To predict the damage location from the waveform response, the Time of Flights (ToF) of A_0 mode and S_0. By finding the displacement-velocity relationship, the damage location can be computed as follows:

$$L_d = ToF\left[\frac{2}{c}\right]^{-1} ( )$$

L_d is the distance between the actuator and the damage and c is the c is the wave speed. ToF is the time it takes for the actuation signal to reach the damage, added to the time for a reflected scattered mode (S_0 or A_0 mode). However, due to the attenuation and distortion of the A_0 signal caused by water and pressure, it becomes challenging to identify. Therefore, we utilized the Time of Flight (ToF) of the S_0 signal to determine the damage location.

To validate the algorithm, we conducted a test by introducing simulated damage located 6 cm away from the actuator towards the sensor. The ToF for the S_0 signal was calculated shown in fig 7.6 to be 2.3 x 10^{-5} s, and the wave speed was determined in section (3.3) to be c = 4418 m/s. According to the equation (), the distance between the actuator and

the damage was calculated to be 5.1 cm, resulting in a 15% error. However, employing multiple sensors allows for more precise localization of the damage.

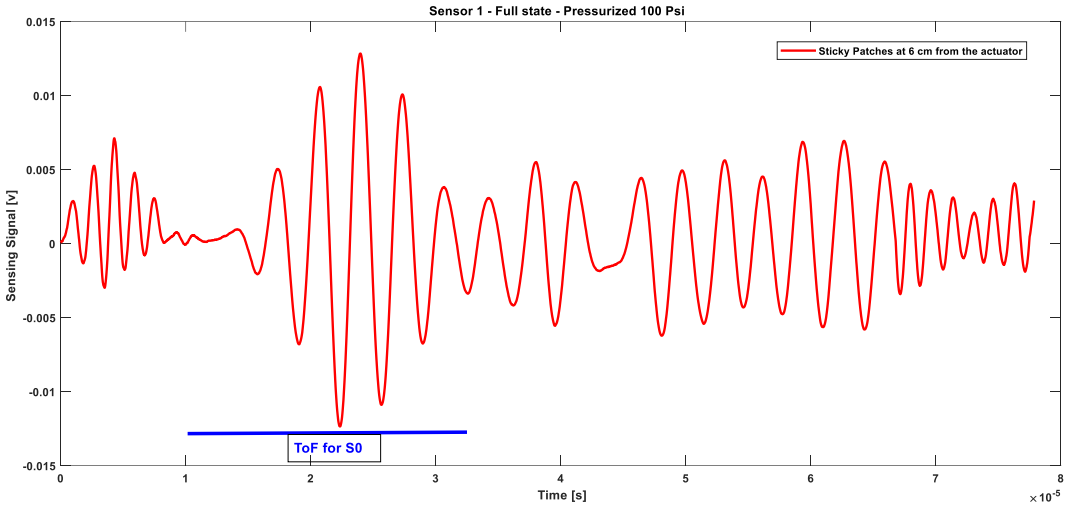

Figure 7. 6: Sensing signal of sensor 1 with the ToF for S_0

7.3 Summary and conclusion

This chapter focuses on creating an algorithm for identifying and pinpointing damage in a pressurized vessel operating at full water state with a pressure of 100 Psi. The algorithm makes use of both the first and second arrival packets. Additionally, the study investigates the ideal number of transducers needed to adequately survey the structure. Assuming the tank is cylindrical, with a diameter (D) of 0.25 m and a height (h) of 0.1 m, giving a total surface area of 0.1767 m2. Each sensor can cover a circular area with a diameter of 0.24 m, equivalent to 0.0452 m2. Thus, 4 sensors are needed to cover the tank, totaling 5 transducers.

The 2D and 3D representation for the transducers coverage for the structure have been set, A 2-D illustration demonstrates sensor coverage based on the minimum number of transducers, while the 3-D representation, enhanced the accuracy of transducers coverages by using 7 transducers (5 sensors and 2 actuators) by keeping the distance between transducers 12 cm and the angle between them being 72°.

The damage algorithm based on the ToF offers two methods for determining damage location: the ToF for S_0 and ToF for A_0 reflection. By analyzing ToF for both modes and considering the displacement-velocity relationship, damage location can be computed. However, due to A_0 signal distortion in water and pressure, ToF of S_0 is preferred. To validate, a test introduced simulated damage 6 cm from the actuator towards the sensor. With S_0 ToF of 2.3 x 10^{-5} s and wave speed (c) of 4418 m/s, damage distance was computed as 5.1 cm, with a 15% error. However, utilizing multiple sensors will improve the localization of the damage precisely.

Chapter8:

Conclusion and future work.

In this chapter, we provide a concise overview of the primary contributions of this thesis and explore potential ways for future research. Furthermore, we delve into the limitations and challenges of the proposed approach, offering a detailed discussion of these aspects.

10.1. Key Contributions and Conclusions

The main key of the thesis is to validate ultrasonic inspection for complex structures. A pressure vessel has been selected as the testbed subject for several reasons. Firstly, it possesses a complex structure comprised of multiple materials, rounded edges, and structural holes. Secondly, the presence of water within the pressure vessel impacts the propagation of waves. Thirdly, examining the ultrasonic inspection under high pressure, this also introduces additional complexity to the propagation of waves. Moreover, a simulated damage has been introduced into the pressure vessel to explore the effects of degradation and corrosion. As a result, the contributions of the thesis can be summarized into three main aspects which examining the ultrasonic inspection for the pressure vessel under varying states (empty and filled with water), varying pressure, and under simulated damage.

The results show that that changing the states of the pressure vessel from empty to full of water will directly affect the second arrivals packets by diminishing the signals and significantly the amplitude of the A_0 mode, these results will help us to decide whether the pressure vessel is empty or full. However, the test goes further to validate the changing of the states under simulated damage, we explore that the introduction of simulated damage on the tank will make the A_0 mode weaker and a reduction in the amplitude has been shown, while the S_0 mode shows slight changes in amplitude. Additionally, a slight angle shift in A_0 between the two signals is observed, indicating the presence of simulated damage.

Three damage index methods based on RMSD, CCD, and NSE were used to measure the difference between baseline signals (empty state) and the measured signals (full water state). Notably, the CCD damage index is sensitive to both empty and full states, as evidenced by consistently higher values in the empty state compared to the full state. RMSD and CCD show sensitivity to state changes caused by wave attenuation.

The effect of the pressure under (changing the states) has been studied, the results show that the pressure significantly reduces the amplitude of symmetrical mode S_0 and slightly affects asymmetrical mode A_0 amplitude at an empty state. Conversely, in a water-filled tank, the pressure primarily affects the antisymmetric mode by reducing its amplitude, while symmetrical mode S_0 remains unchanged.

The effect of the pressure under simulated damage has been studied for both states, results showed a slight decrease in the first and second arrival packets due to simulated damage when the tank was empty, also the results revealed a minor impact on the A_0 signal by decreasing the amplitude when the tank was full of water. various damage index (DI) techniques, namely RMSD, CCD, and NSE, to assess the impact of simulated damage under full water conditions at 100 Psi. The results indicate that the NSE method demonstrates greater sensitivity in detecting simulated damage compared to RMSD and CCD. Additionally, the NSE method enables us to identify which sensors experience complete obstruction of the actuation signal. In contrast, due to their lower values, RMSD and CCD exhibit lower sensitivity to simulated damage.

The optimal number of transducers has been calculated for the structure based on 2- D and 3 D representation, we find that a minimum of 4 transducers are required to cover the structure effectively. The damage algorithm based on the S_0 ToF has been used to determine damage location because A_0 signal distortion in water and pressure. So S_0 is preferred, and we successfully find the location of the damage on the structure with error 15%.

10.2. Future Work

Building a logarithm that can predict the damage location for the simulated damage based on the damage indexes (RMSD, CCD, and NSE), is a big challenge, due to the structure's complexity and the little effect of the simulated damage on the structure. On the other words, The PZTs can sense the simulated damage on the structure but we can't predict the exact location of the simulated damage. RMSD and CCD are not sensitive to simulated damage (sticky patches). While NSE is a little bit sensitive to simulated damage compared with RMSD and CCD. Therefore, trying to find or create a damage index has a high sensing of the distortion and a small reduction of the modes will help to improve the process of localizing the damage.

Another suggested direction for future research entails simulating a real structural defect and exposing it to varying levels of pressure. This testing would provide a good sight for defect detection and localization using ultrasonic inspection. Furthermore, broadening the investigation to include additional modes like S1 and A1 could yield valuable results, and exploring the effect of pressure on S1 and A1 modes could also offer significant benefits.

Expanding the study to investigate the effects of water temperature and dynamic structural conditions, such as utilizing different liquids or gases, or adjusting water flow, would facilitate an analysis of the structure's response to different modes and evaluate the ultrasonic inspection's ability to detect damage under those changing conditions.

Extending the scope of ultrasonic inspection to include pipes made of various materials and with different cross-sections, while studying the influence of temperature, pressure, flow rate, and simulated damage, would contribute to establishing a comprehensive understanding of ultrasonic inspection. This future research would shed light on how signals propagate under these diverse effects, thereby building a physics understanding bases on ultrasonic inspection.

References

[1] J. Fraden, Handbook of Modern Sensors, 4 ed., New York: Springer, 2010.

[2] M. Bahador, A. Zaimbashi and R. Rahgozar, "Three-stage Lamb-wave-based damage localization algorithm in plate-like structures for structural health monitoring applications," *Signal Processing,* 2020.

[3] H. Lamb, "On waves in an elastic plate," *Proceedings of the Royal Society of London, Series A, Containing Papers of a Mathematical and Physical Character, 93, 114-128.,* 1917.

[4] V. Giurgiutiu, Piezoelectric Wafer Active Sensors – PWAS Transducers, Elsevier BV, 2014.

[5] G. Zhang, X. Li, S. Zhang and T. Kundu, "Investigation of frequency-dependent attenuation coefficients for multiple solids using a reliable pulse-echo ultrasonic measurement technique," *Measurement,,* vol. 177, p. 2021.

[6] A. Diogo, B. Moreira, C. A. Gouveia and J. R. Tavares, "A Review of Signal Processing Techniques for Ultrasonic," *MDPI- Metals,* 2022.

[7] V. Gulizzi, P. Rizzo and A. Milazzo, "An integrated structural health monitoring system based on electromechanical impedance and guided ultrasonic waves," *J Civil Struct Health Monit,* vol. 5, no. 2015, p. 337–352, 2015.

[8] M. Meng, Y. Chua, E. Wouterson and C. Ong, "Ultrasonic signal classification and imaging system for composite materials via deep convolutional neural networks," *Neurocomputing, 257, 128–135. https://doi.org/10.1016/j.neucom.2016.11.066,* 2017.

[9] M. M. Nadzri and A. Ahmad, "Design Issues and Challenges of Long-Range Ultrasonic Testing (LRUT) for Pipeline Inspection," *Proceedings of the 12th National Technical Seminar on Unmanned System Technology 2020. Lecture Notes in Electrical*

Engineering, vol 770. Springer, Singapore. https://doi.org/10.1007/978-981-16-2406-3_10.

[10] Y. Sun, Y. Xu, W. Li, Q. Li, X. Ding and W. Huang, "A Lamb Waves Based Ultrasonic System for the Simultaneous Data Communication, Defect Inspection, and Power Transmission," *IEEE Transactions on Industrial Informatics, vol.19, no.12, pp.11418-11429, 2023..*

[11] Y. Lugovtsova and J. Prager, "Structural health monitoring of composite pressure vessels using guided ultrasonic waves," *Insight - Non-Destructive Testing and Condition Monitoring, Volume 60, Number 3, March 2018, pp. 139-144(6).*

[12] L. Fucai, L. Zhiqiang , L. Hongguang and M. Guang, "Propagation of guided waves in pressure vessel," *Wave Motion, Volume 52, January 2015, Pages 216-228.*

[13] K. Yong-Ho, C. Yong-Keun and S. Jung-Il, "The Prediction of Fatigue Damage for Pressure Vessel Materials using Shear Horizontal Ultrasonic Wave," *Journal of the Korean Society for Precision Engineering, Volume 26 Issue 6 / Pages.90-96 / 2009.*

[14] Ting Yu, Weican Guo, Cunjian Miao, Jinyang Zheng and Zhengli Hua, "Study on inserted curved surface coupling phased array ultrasonic inspection of multi-layered steel vessel for high-pressure hydrogen storage," *International Journal of Hydrogen Energy, Volume 46, Issue 35, 20 May 2021, Pages 18433-18444.*

[15] S. Diaz, . L. Pujades , . A. Barbat, Y. Vargas and D. Hidalgo-Leiva, "Energy damage index based on capacity and response spectra," *Engineering Structures,* vol. 152, 2017.

[16] H. Altammar, "Structural Health Monitoring of Laminate Structures Using Shear-Mode Piezoelectric Sensors," University of Wisconsin , Milwaukee, Ph.D Dissertation- 2019.

[17] K.J. Friston a, O. Josephs a, E. Zarahn b, A.P. Ho, "To Smooth or Not to Smooth?: Bias and Efficiency in fMRI Time-Series Analysis," *NeuroImage,* vol. 12, 2002.

[18] Dhaha Dia, Medien Zeghid, Taoufik Saidani, Mohamed, "Multi-level Discrete Wavelet Transform," *Proceedings of the World Congress on Engineering,* vol. 1, 2009.

[19] Qifa Zhou, Sienting Lau, Dawei Wu, K. Kirk Shung, "Piezoelectric films for high frequency ultrasonic transducers in biomedical applications," *Progress in Materials Science,* vol. 56, 2011.

[20] V. Mustafa, A. Chabbaz and R. Hay, "EMAT Generation Of Horizontally Polarized Guided Shear Waves For Ultrasonic Pipe Inspection," in *International Pipeline Conference*, 1998.

[21] L. W. Braile, Seismic Waves and the Slinky, 2001.

[22] H. Altammar and N. Salowitz, "Ultrasonic Inspection of Bonded Metal Laminates Using Internal," *9th European Workshop on Structural Health Monitoring,* 2018.